Journal of Paleontology, 97(2), 2023, p. 454–476

Published by Cambridge University Press
on behalf of The Paleontological Society
0022-3360/23/1937-2337
doi: 10.1017/jpa.2022.98

JOURNAL OF PALEONTOLOGY
A PUBLICATION OF THE Paleontological SOCIETY

First virtual endocast description of an early Miocene representative of Pan-Octodontoidea (Caviomorpha, Hystricognathi) and considerations on the early encephalic evolution in South American rodents

María E. Arnaudo[1]* and Michelle Arnal[1,2]

[1]División Paleontología de Vertebrados, Unidades de Investigación Anexo Museo de La Plata, Facultad de Ciencias Naturales y Museo, Universidad Nacional de La Plata, Av. 122 y 60, B1900FWA La Plata, Argentina <mearnaudo@gmail.com> <michoarnal@gmail.com>
[2]Consejo Nacional de Investigaciones Científicas y Técnicas, CONICET, Argentina.

Abstract.—The study of the cranial endocast provides valuable information to understand the behavior of an organism because it coordinates sensory information and motor functions. In this work, we describe for the first time the anatomy of the encephalon of an early Miocene pan-octodontoid caviomorph rodent (*Prospaniomys priscus* Ameghino, 1902) found in the Argentinean Patagonia, based on a virtual 3D endocast. This fossil rodent has an endocast morphology here considered ancestral for Pan-Octodontoidea and other South American caviomorph lineages, i.e., an encephalon with anteroposteriorly aligned elements, mesencephalon dorsally exposed, well-developed vermis of the cerebellum, and rhombic cerebral hemispheres with well-developed temporal lobes. *Prospaniomys* Ameghino, 1902 also has relatively small olfactory bulbs, large paraflocculi of the cerebellum, and low endocranial volume and degree of neocorticalization. Its encephalization quotient is low compared with Paleogene North American and European noncaviomorph rodents, but slightly higher than in several late early and late Miocene caviomorphs. Paleoneurological anatomical information supports the hypothesis that *Prospaniomys* was a generalist caviomorph rodent with terrestrial habits and enhanced low-frequency auditory specializations. The scarce paleoneurological information indicates that several endocast characters in caviomorph rodents could change with ecological pressures. This work sheds light on the anatomy and evolution of several paleoneurological aspects of this particular group of South American rodents.

Introduction

The New World hystricognath rodents (= Caviomorpha) are a particular group of mammals characterized by being morphologically and ecologically very diverse (Wood, 1955; Patton et al., 2015; Upham and Patterson, 2015; Vucetich et al., 2015a). They reached South America during the Eocene and rapidly evolved into several lineages (Poux et al., 2006; Antoine et al., 2012; Arnal and Vucetich, 2015; Boivin et al., 2019). The main reasons for their impressive evolutionary history seem related to the successful paleobiology of these rodents occupying empty niches and evolving on an island continent during most of the Cenozoic (Upham and Patterson, 2015; Vucetich et al., 2015a; Boivin et al., 2018; Arnal et al., 2020, 2022). Fossil and living caviomorphs have exploited a wide array of ecological niches, inhabiting almost all environments and having generalist, arboreal, fossorial, subterranean, and aquatic habits (Verzi et al., 2010; Candela et al., 2012; Álvarez and Arnal, 2015; Patton et al., 2015; Álvarez and Ercoli, 2017; Kerber et al., 2022). In addition, they have been morphologically very diverse and have acquired a great disparity of sizes (from small to the largest rodents that ever lived on Earth) (Rinderknecht and Blanco, 2008; Vucetich et al., 2015a). Caviomorphs are grouped into four main clades (i.e., Pan-Octodontoidea sensu Arnal and Vucetich, 2015; Chinchilloidea; Cavioidea; and Erethizontoidea) and several independent fossil lineages not included in any of these four main groups (Antoine et al., 2012; Arnal and Vucetich, 2015; Patton et al., 2015; Upham and Patterson, 2015; Boivin et al., 2019; Fig. 1).

Prospaniomys priscus Ameghino, 1902 is a monospecific genus of pan-octodontoid caviomorph from the early Miocene (~20–21 Ma) of the Argentinean Patagonia (Ameghino, 1902; Vucetich et al., 2010a; Arnal and Kramarz, 2011; Arnal, 2012). Pan-octodontoids represent the earliest caviomorph lineage to differentiate and their fossil record is very abundant (Vucetich et al., 2010a, 2015a). *Prospaniomys* Ameghino, 1902 is a stem pan-octodontoid (Fig. 1), which means that its morphology could be interpreted as ancestral to crown pan-octodontoids, the clade that includes living pan-octodontoids (Fig. 1). Only one almost-complete cranium of *Prospaniomys* is known (Arnal and Kramarz, 2011; Arnal, 2012; Fig. 2.1, 2.2). It has a particular and interesting cranial morphology with generalized cheek teeth (brachydont and bunolophont) and a supposedly derived basicranium (e.g., large auditory bullae) (Arnal and Kramarz, 2011; Arnaudo et al., 2020; Fig. 2.1–2.3). Owing to this striking morphology, some works have focused on different aspects of the paleobiology of this taxon. Álvarez and Arnal (2015) reconstructed the head muscles and studied the craniomandibular shape variation and concluded that *Prospaniomys* had generalized habits and a diet based on soft, non-abrasive items. Arnaudo et al. (2020) studied its auditory region

*Corresponding author.

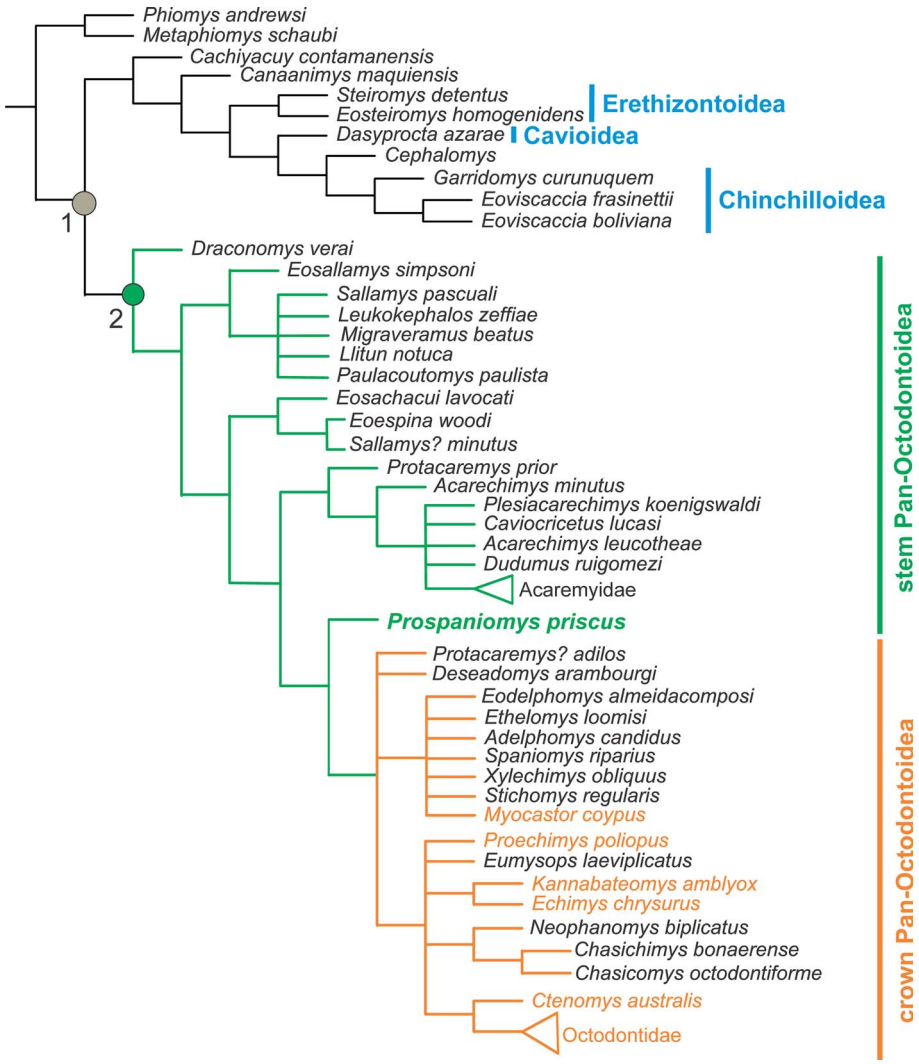

Figure 1. Phylogeny from Arnal and Vucetich (2015) showing the relationships of *Prospaniomys* (green font) within Pan-Octodontoidea, and the relationships of the four main caviomorph clades (i.e., Pan-Octodontoidea, Chinchilloidea, Cavioidea, Erethizontoidea) and other fossil lineages (e.g., *Cephalomys* Ameghino, 1897, *Cachiyacuy* Antoine et al., 2012; sensu Arnal and Vucetich, 2015). 1 = Caviomorpha; 2 = Pan-Octodontoidea; green = stem Pan-Octodontoidea; orange = crown Pan-Octodontoidea (names in orange refers to living crown pan-octodontoids). Taxa not otherwise mentioned in the text are: *Acarechimys leucotheae* Vucetich et al., 2015b; *Acarechimys minutus* (Ameghino, 1887); *Adelphomys candidus* Ameghino, 1887; *Cachiyacuy contamanensis* Antoine et al., 2012; *Canaanimys maquiensis* Antoine et al., 2012; *Caviocricetus lucasi* Vucetich and Verzi, 1996; *Chasichimys bonaerense* Pascual, 1967; *Chasicomys octodontiforme* Pascual, 1967; *Ctenomys australis* Rusconi, 1934; *Dasyprocta azarae* Lichtenstein, 1823; *Deseadomys arambourgi* Wood and Patterson, 1959; *Draconomys verai* Vucetich et al., 2010b; *Dudumus ruigomezi* Arnal et al., 2014; *Echimys chrysurus* Zimmermann, 1780; *Eodelphomys almeidacomposi* Frailey and Cambell, 2004; *Eoespina woodi* Frailey and Cambell, 2004; *Eosachacui lavocati* Frailey and Cambell, 2004; *Eosallamys simpsoni* Frailey and Cambell, 2004; *Eosteiromys homogenidens* Ameghino, 1902; *Eoviscaccia boliviana* Vucetich, 1989; *Eoviscaccia frasinettii* Bertrand et al., 2012; *Ethelomys loomisi* (Wood and Patterson, 1959); *Eumysops laeviplicatus* Ameghino, 1888; *Garridomys curunuquem* Kramarz et al. 2013; *Kannabateomys amblyox* Wagner, 1845; *Leukokephalos zeffiae* Vucetich et al., 2015b; *Llitun notuca* Vucetich et al., 2015b; *Metaphiomys schaubi* Wood, 1968; *Migraveramus beatus* Patterson and Wood, 1982; *Neopahnomys biplicatus* Roverето, 1914; *Paulacoutomys paulista* Vucetich et al. 1993; *Phiomys andrewsi* Osborn, 1908; *Plesiacarechimys koenigswaldi* Vucetich and Vieytes, 2006; *Proechimys poliopus* Osgood, 1914; *Protacaremys adilos* Vucetich et al., 2015b; *Protacaremys prior* Ameghino, 1902; *Sallamys minutus* Vucetich and Ribeiro, 2003; *Sallamys pascuali* Hoffstetter and Lavocat, 1970; *Spaniomys riparius* Ameghino, 1887; *Steiromys detentus* Ameghino, 1887; *Stichomys regularis* Ameghino, 1887; *Xylechimys obliquus* Patterson and Pascual, 1968.

and concluded that *Prospaniomys*, and pan-octodontoids in general, evolved adaptations to low-frequency hearing since the early Miocene. In this context, the integration of ear information with that provided by the cranial endocast is of primary importance to study the sensitivity system of this fossil taxon. The encephalon provides valuable information to understand the behavior of an organism because it coordinates sensory information and motor functions (Liem et al., 2001; Evans and de Lahunta, 2013). Through the study of the sensory system, it is possible to infer several paleobiological aspects (Köhler and Moyà-Solà, 2004; Bertrand et al., 2018; Fernández-Monescillo et al., 2019).

In most mammals, the encephalon fills the cranial cavity, leaving impressions of structures on the inner part of the cranium (Jerison, 1973). Within the braincase are housed different structures and cavities of the encephalon, bounded anteriorly by the cribriform plate and posteriorly by the occipital complex (Liem et al., 2001; Macrini et al., 2006). Other soft anatomical structures also leave their impressions on the braincase: meninges, blood and lymphatic vessels (as the dural sinuses, e.g.,

https://doi.org/10.1017/jpa.2022.98 Published online by Cambridge University Press

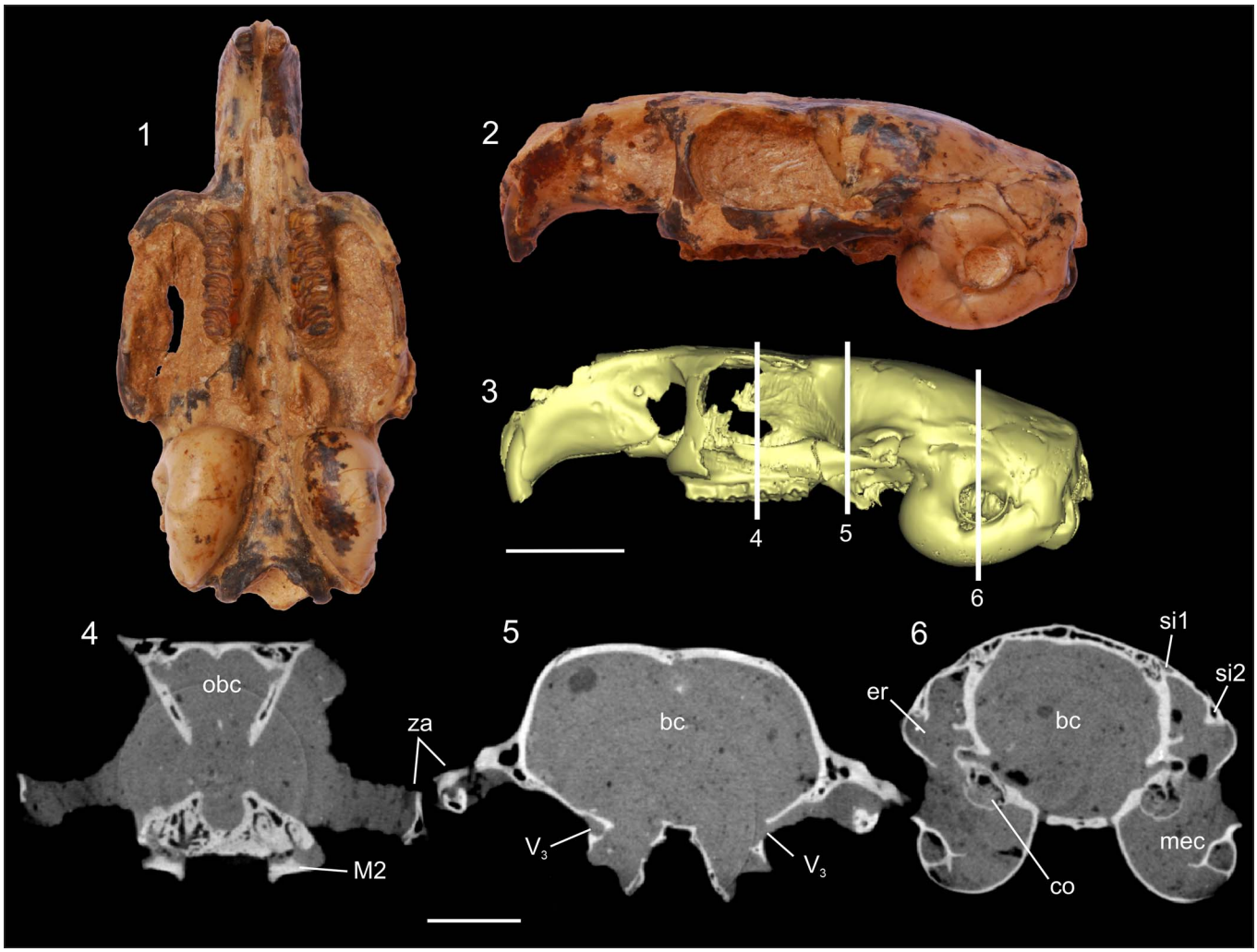

Figure 2. Studied cranium of *Prospaniomys priscus* (MACN-PV CH1913): (**1, 2**) ventral and left lateral views, respectively; (**3**) 3D surface reconstruction in left lateral view showing the three points from the X-ray tomography slices (**4–6**) (note the absence of the surrounding sediment in this 3D reconstruction); (**4–6**) X-ray computed tomography slices at the level of the orbital, postorbital, and auditory regions, respectively. bc = brain cavity; co = cochlea; er = epitympanic recess; M2 = upper second molar; mec = middle ear cavity; obc = olfactory bulbs cavity; si1 = sinus 1; si2 = sinus 2; V_3 = passage for masseteric and buccinator branches of mandibular branch of trigeminus nerve; za = zygomatic arch. Scale bars = 10 mm (**1–3**); 5 mm (**4–6**).

longitudinal fissure, transverse sinus, sigmoid sinus, small veins, and arteries), and cranial nerves (Macrini et al., 2007). In fossil taxa, soft tissues are not preserved, but the cranial cavity can be filled, forming a three-dimensional (3D) representation of the space in the cavity (i.e., cranial endocasts; Macrini et al., 2007). Mammal cranial endocasts permit the acquisition of excellent representations of the external anatomy of the encephalon (Radinsky, 1968) to obtain reliable linear and volumetric measures (e.g., Radinsky, 1968; Quiroga, 1988; Dozo, 1997a, b; Dozo et al., 2004; Macrini et al., 2006, 2007; Bertrand and Silcox, 2016; Dozo and Martínez, 2016; Ferreira et al., 2020, 2021). There are different types of endocasts: (1) natural endocasts, in which the surrounding matrix fills the cranial cavity (Dechaseaux, 1958; Dozo et al., 2004; Bertrand and Silcox, 2016; Madozzo-Jaén, 2019; Ferreira et al., 2020); (2) latex endocasts, made from a complex process only possible in empty cranial cavities (Dozo, 1997a, b); and (3) 3D digital endocasts, obtained through the use of CT scans or MicroCT scans (Bertrand and Silcox, 2016; Bertrand et al., 2016b, 2017, 2018, 2019; Ferreira et al., 2020, 2021). Digital endocasts are the best noninvasive way of studying braincases because they allow the acquisition of high-quality virtual 3D models of intracranial cavities without damaging the material.

The discipline that studies the neuroanatomy of extinct taxa is known as paleoneurology. Paleoneurological information for rodents in general and caviomorphs in particular is scarce. The oldest and most representative works are those of Dechaseaux (1958) and Pilleri et al., (1984) who included brief descriptions of a few fossil rodents. Dozo (1997b) and Dozo et al., (2004) described natural endocasts of Cephalomyidae gen. indet. sp. indet. and of the erethizontid (= erethizontoid) *Hypsosteiromys* Patterson, 1958, respectively, both from the early Miocene of the Argentinean Patagonia. Using latex, Dozo (1997a) studied the cranial endocast of the cavioid *Dolicavia* Ameghino, 1916 from the early Pliocene of Buenos Aires Province, Argentina. Madozzo-Jaén (2019) briefly described part of a natural endocast of *Prodolichotis prisca* (Rovereto, 1914) from the late Miocene–early Pliocene of northwestern Argentina. In the last

https://doi.org/10.1017/jpa.2022.98 Published online by Cambridge University Press

years, with the incorporation of virtual 3D digital models, paleoneurological works have become more abundant. Bertrand and collaborators studied cranial endocasts of several Paleogene ischyromyid rodents and of extinct sciuroid rodents (Bertrand and Silcox, 2016; Bertrand et al., 2016b, 2017, 2018, 2019). For Caviomorpha, Ferreira et al. (2020) described the virtual endocast of the late Miocene chinchilloid *Neoepiblema* Ameghino, 1889 from Brazil, and Ferreira et al. (2021) described several virtual endocasts of living cavioids. In these works, endocasts of other caviomorphs were reconstructed or figured (e.g., Dozo, 1997b; Dozo et al., 2004; Madozzo-Jaén, 2019; Ferreira et al., 2020, 2021), but the neuroanatomy of pan-octodontoids remains practically unknown.

Here, we describe for the first time the anatomy of the cranial endocast of an early Miocene stem pan-octodontoid based on a virtual 3D endocast. The basal phylogenetic position of *Prospaniomys* within Pan-Octodontoidea (Fig. 1) sheds light on the earlier endocranial anatomy of the group, and allows anatomical comparisons with other extinct and living caviomorphs (Pilleri et al., 1984; Dozo, 1997a, b; Dozo et al., 2004; Madozzo-Jaén, 2019; Ferreira et al., 2020, 2021), as well as other fossil rodents (e.g., Dechaseaux, 1958; Pilleri et al., 1984; Bertrand and Silcox, 2016; Bertrand et al., 2016b, 2017, 2018, 2019). We also describe and mention different aspects of the cranial circulatory system and cranial foramina. The results obtained here allow evaluation of different evolutionary and paleoecological aspects of pan-octodontoids in particular, as well as general paleoneurological considerations about caviomorphs.

Materials and methods

We describe the first complete virtual endocast of *Prospaniomys priscus* based on the only known cranium of this taxon (MACN-PV CH1913). MACN-PV CH1913 was originally described as *Prospaniomys* cf. *P. priscus* (see Arnal and Kramarz, 2011). Subsequently, Arnal (2012) performed a taxonomic revision of the genus and recognized this cranium as *Prospaniomys priscus*. The almost-complete cranium of the fossil taxon has outstanding preservation and, therefore, an almost complete and detailed virtual endocast could be realized (Fig. 2). MACN-PV CH1913 was collected in early Miocene levels (Arquitanian–Burdigalian; ~20–21 Ma) of the Sarmiento Formation exposed at Pampa de Gan Gan, Chubut Province, Argentina (Fleagle and Bown, 1983; Arnal and Kramarz, 2011). The cranium is externally clean, but is filled with a hard matrix inside and in the orbital region (Fig. 2).

Descriptions are based on osteological features, which permit us to infer the existence of the described soft structures. For general terminology of the encephalon and its portions, we follow the English equivalents of terms used in the sixth edition of the Nomina Anatomica Veterinaria (2017). This is to use accurate anatomical terminology. Other cephalic nomenclature follows Dozo (1997a, b) and Ferreira et al., (2021, and references therein) (Fig. 3.1). Cranial nomenclature follows Hill (1935), Wahlert (1985), and International Committee on Veterinary Gross Anatomical Nomenclature (2017) (Fig. 3.2). We have made reference to other literature in certain parts of the description only when referring to structures differently interpreted from the above-mentioned works. Anatomical terms and their abbreviations are summarized in Figure 3.

The specimen of *Prospaniomys* was scanned using high-resolution microtomography (μCT) at Y-TEC, Berisso, Buenos Aires Province, Argentina. The cranium was completely scanned in 2018, but for this work, only the encephalic region was segmented. MicroCT data were acquired using a Sky-Scan1173 scanner; a total of 1,105 slices were obtained with an interslice spacing and interpixel distance (X = Y = Z) of 0.04716 mm, a field of view of 5.29 cm, and energy parameters of 120 kV and 66 mAs. The segmentation process and visualization of the slices were done using the free software 3D Slicer v4.11 (Fedorov et al., 2012). The virtual endocranial cavity was manually segmented. The segmentation and virtual 3D models were carried out using the module "Segment Editor" of 3D Slicer. The surface renderings of the endocasts described in this paper are available on Dryad (www.datadryad.org). Cranial bones have a different contrast with respect to the surrounding matrix (Fig. 2.4–2.6), which allows them to separate one from another. Descriptions of soft encephalic structures were performed only from the virtual 3D endocasts, whereas descriptions of nerves, blood vessels, and foramina were taken into account in the CT Scans, 3D reconstructions, and the specimens. When necessary, CT slices of transverse planes were used to obtain better understanding of different structures (Fig. 2.4–2.6). This was the case, for example, for identifying fissures from sinuses (e.g., fissura transversa from the transverse sinus). A fissura is a deep sulcus over the surface of the encephalon that could be the space occupied by the meninges (e.g., longitudinal fissure) or the result of convolutions owing to the enlargement of the cerebrum and cerebellum (Liem et al., 2001; Kardong, 2012). A sinus is evidenced as a protuberance in the surface of the endocast that is the result of a channel that protrudes over the 3D cranial endocast (Liem et al., 2001; Kardong, 2012). The 3D cranial endocast of *Prospaniomys* is shown in Figure 4.

The virtual cranial endocast of *Prospaniomys* was compared with natural and virtual caviomorph endocasts from the literature (Pilleri et al., 1984; Dozo, 1997a, b; Dozo et al., 2004; Madozzo-Jaén, 2019; Ferreira et al., 2020, 2021; Fig. 5). In addition, virtual endocasts of noncaviomorph rodents (Ischyromyidae sensu Korth, 1994) from Paleogene ages of North America were used for comparisons following the literature: *Paramys* Leidy, 1871, *Notoparamys* Korth, 1984, and *Pseudotomus* Cope, 1872 (Paramyinae) from the early–late Eocene; *Reithroparamys* Matthew, 1920 and *Rapamys* Wilson, 1940 (Reithroparamyinae) from the early–late Eocene; *Ischyromys* Leidy, 1856 (Ischyromyinae) from the early Eocene–early Oligocene; and the oldest recorded squirrel, *Cedromus wilsoni* Korth and Emry, 1991, from the early Oligocene (Bertrand and Silcox, 2016; Bertrand et al., 2016b, 2017, 2018, 2019). These taxa were included in the comparisons because they have several ancestral traits that deserve comparison with the fossil caviomorphs to reconstruct possible ancestral character states.

Measurements.—The volume of the total cranial endocast, of the olfactory bulbs and paraflocculi, and linear measurements were obtained using the software 3D Slicer; all values are listed in Table 1. The volume of the olfactory bulbs and

https://doi.org/10.1017/jpa.2022.98 Published online by Cambridge University Press

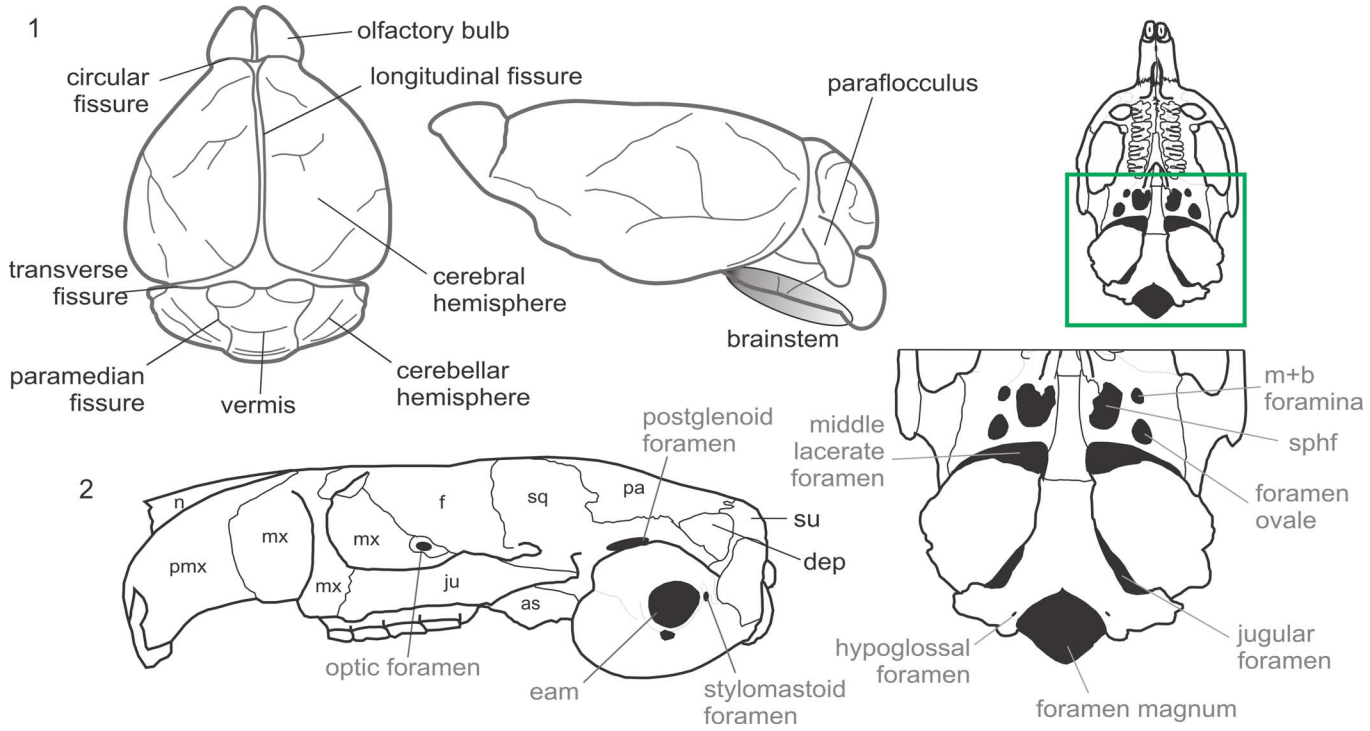

Figure 3. (**1**) Encephalic diagram of a generalized mammal showing the main structures mentioned in the text, following Dozo (1997a, b), the sixth edition of the NAV (International Committee on Veterinary Gross Anatomical Nomenclature, 2017), and Ferreira et al. (2021, and references therein). (**2**) Osteological nomenclature of bones (black font) and foramina (gray font) following Hill (1935), Wahlert (1985), and the sixth edition of the NAV (International Committee on Veterinary Gross Anatomical Nomenclature, 2017). as = alisphenoid; dep = dorsal exposition of petrosal; eam = external acoustic meatus; f = frontal; ju = jugal; m+b = masticatory + buccinator; mx = maxillary; n = nasal; pa = parietal; pmx = premaxillary; sphf = sphenorbital fissure; sq = squamosal; su = supraoccipital.

paraflocculi were obtained by isolating those structures following Macrini et al. (2006) and resegmenting them with different labels. Linear measurements were obtained with the "Ruler" tool from the "Mouse Interaction" toolbar (following Bertrand and Silcox, 2016), whereas volumetric measurements were shown in the label "Volume" in the "Information" panel of the "Models" module.

Ratios between the linear measures, the surface area of the neocortex with respect to the total surface area of the endocast, and volumes of different parts of the endocast were calculated to make comparisons (Table 1). In Table 1, we also included measurements available for the taxa used in the comparisons (see below).

The neocortical area ratio (neocortical surface area / total endocast surface area, NS/TS) of *Prospaniomys* was calculated (Table 1). The surface of the neocortex (NS) was estimated using the tool "Closed curve" of the module "Markups." We follow Jerison (2012) and selected the neocortical area of one side, which is delimited anteriorly by the entry of the olfactory tract, dorsally by the longitudinal fissure, ventrally by the rhinal sulcus, and posteriorly by the boundary between the cerebrum and cerebellum. At the posterior border, we excluded the ventral region of the endocast, posterior to the piriform lobe. Once we obtained this measure, we multiplied it by 2. The complete surface area of the endocast (TS) of *Prospaniomys* was obtained in the label "Surface area," also in the "Information" panel of the module "Models."

Boxplots and regression analyses.—To make our results more comprehensible, we generated boxplots with the information obtained from the volume of the olfactory bulbs and paraflocculi, and the neocortical area ratio (Fig. 6; Supplementary data); we also generated linear regression plots with the volume and masses of the olfactory bulbs and paraflocculi and the area of the neocortex with respect to the total endocranial area of all taxa (Fig. 7; Supplementary data). Finally, we generated boxplots for the three encephalization quotient (EQ) equations and a regression plot between endocranial mass and body mass of all specimens for which data were available (Fig. 8). Linear regression models followed the Ordinary Least Square (OLS) method. Assumptions of normality and homoscedasticity were tested to achieve the requirements of the model (see Supplementary data). The data used in these analyses (slope, intercept, and p-values obtained from regression analyses) are found in the Supplementary Data. All graphs were obtained using the free software PAST v4.10 (Hammer et al., 2001).

Encephalization quotients.—The encephalization quotient is a dimensionless measure of the ratio between the real endocranial size of a specimen and the expected endocranial size for an average mammal of the same body size (Jerison, 1973; Gingerich and Gunnel, 2005). It allows comparisons of relative endocranial sizes between species of different body masses. Three different equations were used (i.e., Jerison, 1973; Eisenberg, 1981; Pilleri et al., 1984) to be able to compare all of the information available in the bibliography (but see discussion by Bertrand et al., 2016b). To calculate the encephalization quotient, two parameters are necessary:

https://doi.org/10.1017/jpa.2022.98 Published online by Cambridge University Press

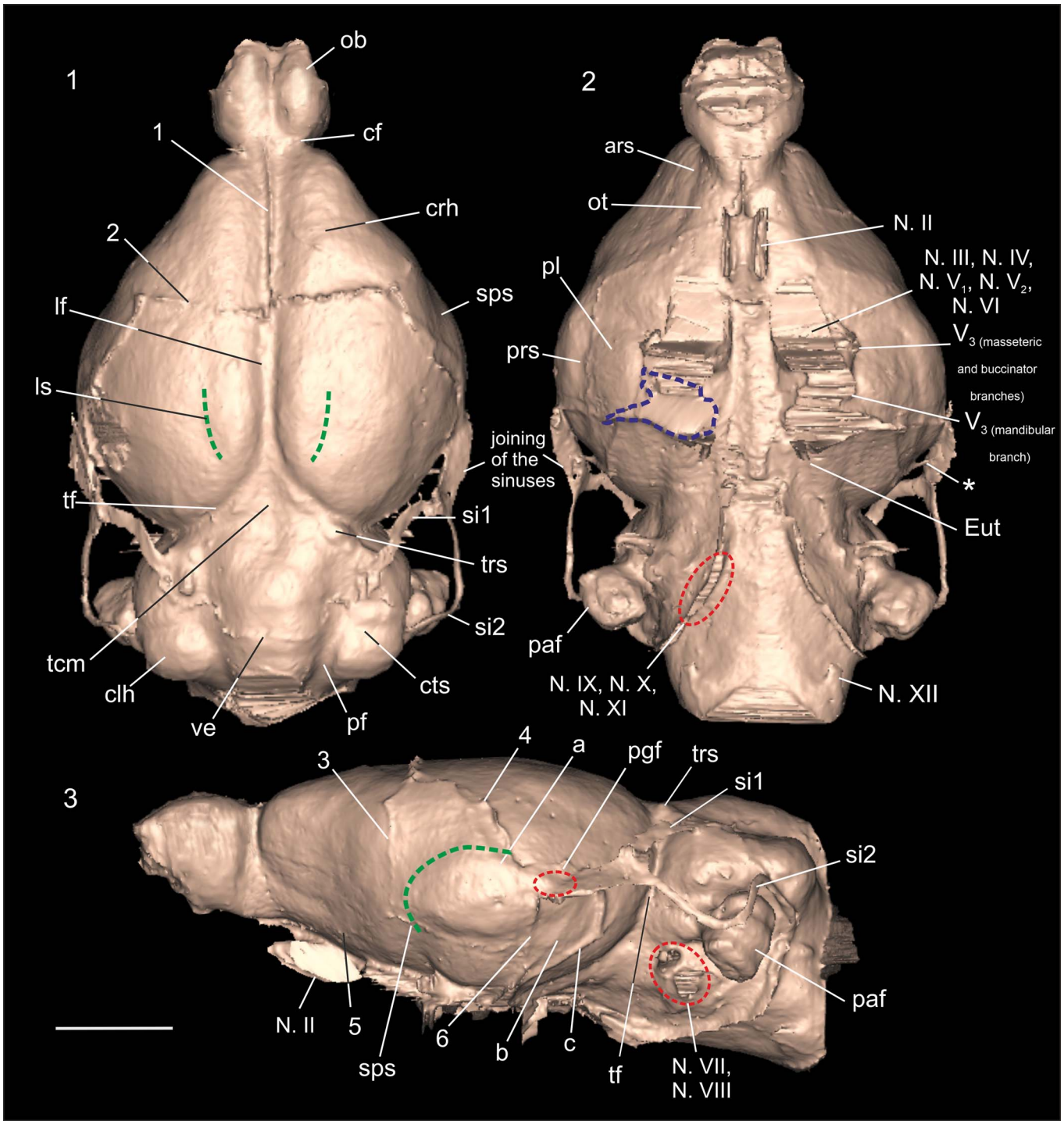

Figure 4. Endocranial morphology of *Prospaniomys priscus* (3D virtual endocast of MACN-PV CH1913): (**1**) dorsal view; (**2**) ventral view; (**3**) right lateral view (mirrored). ars = anterior rhinal sulcus; cf = circular fissure; clh = cerebellar hemisphere; crh = cerebral hemisphere; cts = cerebellar transverse sulcus; Eut = aperture of the Eustachian tube; lf = longitudinal fissure; ls = lateral sulcus; N. II = optic nerve (= optic tract); N. III = oculomotor nerve; N. IV = trochlear nerve; N. V_1 = deep ophthalmic branch of trigeminus nerve; N. V_2 = maxillary branch of trigeminus nerve; N. V_3 = mandibular branch of trigeminus nerve; N. VI = abducens nerve; N. VII = facial nerve; N. VIII = vestibulocochlear nerve; N. IX = glossopharyngeal nerve; N. X = vagus nerve; N. XI = accessory nerve; N. XII = hypoglossal nerve; ob = olfactory bulbs; ot = olfactory tract; paf = paraflocculus; pf = paramedian fissure; pgf = postglenoid foramen; pl = piriform lobe; prs = posterior rhinal sulcus; si1 = sinus 1; si2 = sinus 2; sps = suprasylvian sulcus; tcm = tectum of mesencephalon; tf = transverse fissure; trs = transverse sinus; ve = vermis; 1 = suture between frontal bones; 2 = suture between frontal and parietal bones; 3 = suture between frontal and squamosal bones; 4 = suture between squamosal and parietal bones; 5 = suture between frontal and orbitosphenoid bones; 6 = sutures between auditory bulla with squamosal and alisphenoid bones; a, b, c = vascular impressions (see text for details); * = vessel c, which passes through a small foramen in anterodorsal region of cerebellar face of the petrosal. The green dashed lines mark the position of sulci on the surface of the endocast. The red dashed circles indicate different foramina: the jugular foramen in ventral view for the exit of nerves IX, X, and XI; the postglenoid foramen and the internal acoustic meatus for the passage of nerves VII and VIII in lateral view. The blue dashed line shows the area that could not be clearly reconstructed. It is marked only on the right side, but the same occurred on the left side of the endocast. Scale bar = 5 mm.

https://doi.org/10.1017/jpa.2022.98 Published online by Cambridge University Press

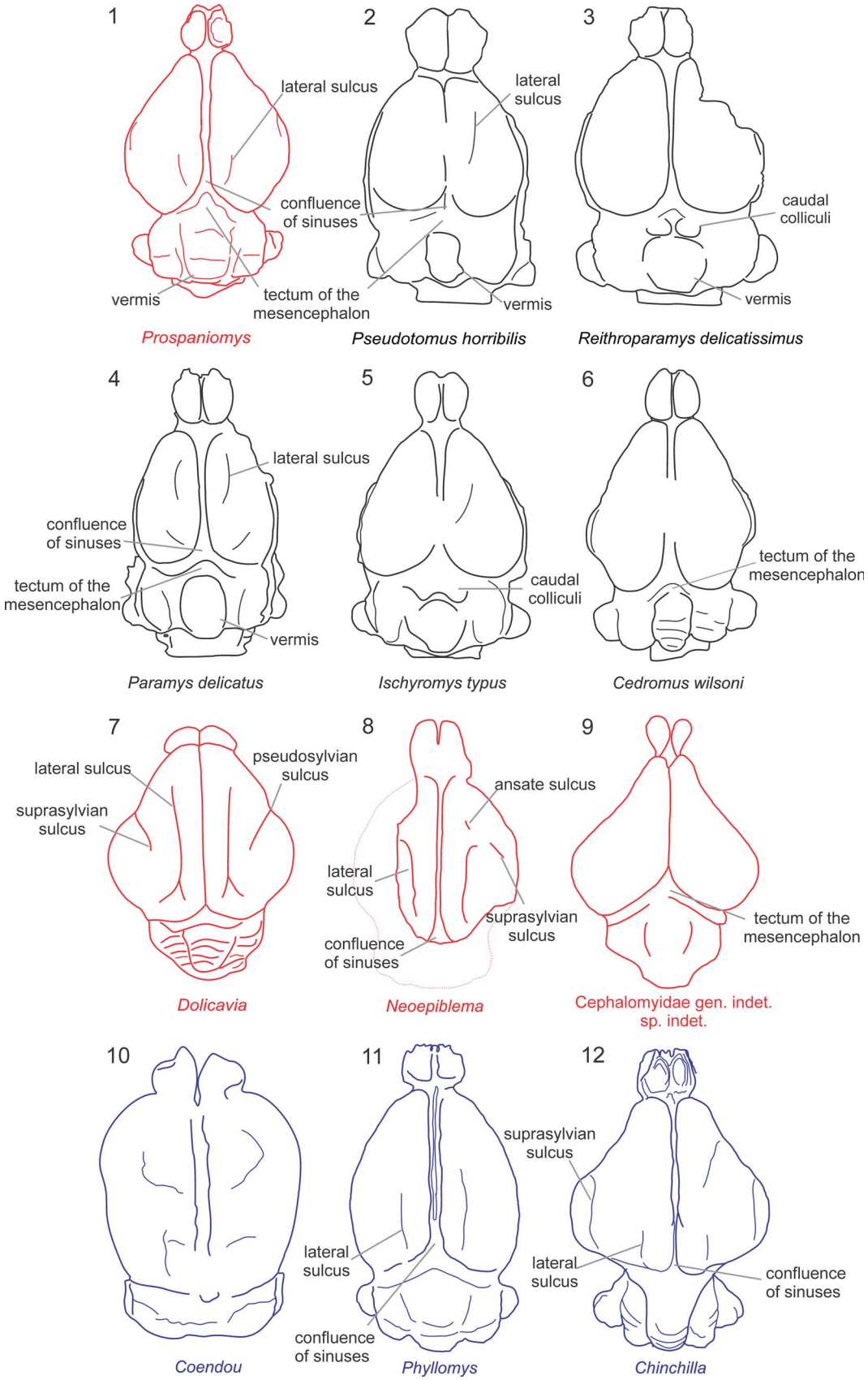

Figure 5. Endocranial diagrams in dorsal view of several rodents used in the comparisons. (**1, 7–9**) encephalons of fossil caviomorphs (red), (**10–12**) of living caviomorphs (blue), (**2–6**) of fossil noncaviomorph rodents (black). Drawings based on figures by Dozo (1997a, b), Bertrand and Silcox (2016), Bertrand et al. (2016b, 2017, 2019), and Ferreira et al. (2021).

https://doi.org/10.1017/jpa.2022.98 Published online by Cambridge University Press

Table 1. Comparisons of different encephalic measurements, including new values taken for *Prospaniomys* and available information for other rodents. Length, width, and height measurements are in mm; area values are in mm^2; volume values are in mm^3. CLL = cerebellum length; CLL/EL = percentage of cerebellum length; CLW = cerebellum width; CLW/EW = percentage of cerebellum width; CRL = cerebrum length; CRL/EL = percentage of cerebrum length; CRW = cerebrum width; EL = endocast length; EV = total endocast volume; NS = neocortical surface area; NS/TS = percentage of the neocortical surface area relative to the total endocast surface area; OBH = olfactory bulbs high; OBL = olfactory bulbs length; OBL/EL = percentage of olfactory bulbs length; OBV = olfactory bulbs volume; OBV/EV = percentage of the olfactory bulbs relative to the total endocast volume; OBW = olfactory bulbs width; OBW/EW = percentage of the olfactory bulbs width; TPV = total paraflocculi volume; TPV/EV = percentage of the paraflocculi relative to the total endocast volume; TS = total endocast surface area; 1 = Ferreira et al. (2020); 2 = Bertrand and Silcox (2016); 3 = Ferreira et al. (2021); 4 = Bertrand et al. (2016); 5 = Bertrand et al. (2017); 6 = Bertrand et al. (2019); * = calculated in this work; † = fossil species. The paraflocular volume of *Prospaniomys* was obtained from Arnaudo et al. (2020). EV for caviomorphs was calculated using the available information from Ferreira et al. (2020).

	Taxon	EL	EV	OBV	OBV/EV	OBL	OBL/EL	OBW	OBW/EW	OBH	CRL
Pan-Octodontoidea	†*Prospaniomys priscus*	27.2*	2,425.8*	63.6*	2.6*	3.84*	14.1*	5.3*	30.8*	4.5*	16.0*
	Phyllomys dasythrix [1]	30.4	2,573.77	75.52	2.93*	4.19	13.78	6.22	36.65	4.46	17.40
	Myocastor coypus [1]	50.38	16,432.1	312.43	1.90*	6.67	13.24	12.53	40.35	7.68	31.90
Erethizontoidea	*Coendou spinosus* [1]	44.01	13,831.53	308.58	2.23*	6.41	14.56	14.31	47.17	8.51	28.33
Cavioidea	†*Neoreomys australis* [1]	54.65	13,208.44	436.48	3.30*	10.20	18.66	9.18	29.74	8.64	30.49
	Cavia porcellus [1]	61.55	4,532.05	124.45	2.74*	10.64	15.0	13.05	33.69	5.56	23.03
	Cavia aperea [3]	-	4,091.78*	144	3.52	-	-	-	-	-	-
	Dolichotis patagonum [3]	-	29,598.64*	557	1.87	-	-	-	-	-	-
	Hydrochoerus hydrochaeris [3]	-	95,022	1900	2.09	-	-	-	-	-	-
	Hydrochoerus hydrochaeris[1]	93.44	94,746.94	2,278.62	2.40*	11.26	12.05	25.56	40.60	16.48	58.46
	Kerodon (*Galea*) *spixii* [3]	-	3,746.95*	149	3.99	-	-	-	-	-	-
	Kerodon rupestris [3]	-	5,929.57*	117	2.06	-	-	-	-	-	-
	Dasyprocta sp.[1]	61.55	23,980.98	865.35	3.60*	10.64	17.28	13.05	35.07	8.77	38.46
	Dasyprocta leporina [3]		24,088.85*	792	3.27						
	Dasyprocta variegata [3]	-	23,621.17*	786	3.31	-	-	-	-	-	-
Chinchilloidea	*Dinomys branickii* [1]	70.73	43,502.22	1,073.78	2.46	9.14	12.92	15.74	34.97	7.58	45.96
	†*Neoepiblema acreensis* [1]	82.88	49,682.06	-	-	11.15	13.45	13.34	23.87	6.34	54.43
	Cuniculus paca [3]	-	45,552.4*	1076	2.36	-	-	-	-	-	-
	Chinchilla lanigera [1]	38.84	5,669.75	112.40	1.98*	5.05	13.0	7.44	29.76	5.14	22.85
	Lagostomus maximus [1]	56.23	17,803.59	267.24	1.50*	7.36	13.09	9.27	23.77	6.46	34.76
Paleogene non- caviomorph rodents	†*Ischyromys typus* (ROMV 1007)[2]	40.55	5,578.07	180.09	3.23	7.24	17.85	7.12	30.20	5.75	20.96
	† *Ischyromys typus* (AMNH 12252)[2]	39.51	5934.55	218.46	3.68	5.99	15.16	7.29	36.34	6.43	18.77
	† *Ischyromys typus* (AMNH F:AM 144638)[2]	40.43	7276.91	229.12	3.15	7.14	17.66	7.73	36.05	6.72	20.43
	†*Paramys copei* [4]	45.82	7526.65	455.45	6.05	10.11	22.06	9.36	44.85	7.95	21.05
	†*Paramys delicatus* [4]	50.54	12565.40	595.51	4.74	10.17	20.12	11.15	43.50	8.68	23.27
	†*Cedromus wilsoni* [5]	31.98	3609.87	106.97	2.96	5.70	17.82	6.17	47.68	5.31	18.61
	†*Pseudotomus horribilis* [6]	54.38	15188.20	808.92	5.33	11.76	21.63	16.49	51.35	11.42	26.42
	†*Pseudotomus oweni* [6]	51.72	12063.00	717.06	5.94	10.20	19.72	12.49	24.30	10.61	28.20
	†*Pseudotomus petersoni* [6]	51.81	17014.90	704.34	4.14	9.15	17.66	15.43	49.06	10.03	28.33
	†*Pseudotomus hians* [6]	47.78	13679.10	743.20	5.43	7.82	16.37	15.82	48.92	9.51	23.83
	†*Reithroparamys delicatissimus* Leidy, 1871[6]	36.08	-	-		5.62	15.58	7.49	34.12	6.14	17.67
	†*Rapamys atramontis* (AMNH 128706)[6]	41.49	7109.97	224.62	3.16	7.63	18.39	7.99	36.04	6.02	21.58
	†*Rapamys atramontis* (AMNH 128704)[6]	39.48	6006.47	226.06	3.76	7.71	19.53	8.17	36.74	6.11	19.99

	Taxon	CRW	CRL/EL	NS	TS	NS/TS	CLL	CLL/EL	CLW	CLW/CRW	TPV	TPV/EV
Pan-Octodontoidea	†*Prospaniomys priscus*	17.2*	58.82*	242.4*	1,397.6*	17.34*	6.8*	24.9*	11.9*	69.2*	36	1.48*
	Phyllomys dasythrix[1]	16.97	57.24	-	-	-	5.91	19.44	12.47	73.48	-	-
	Myocastor coypus[1]	31.05	63.32	-	-	-	9.26	18.38	20.53	66.12	-	-
Erethizontoidea	*Coendou spinosus*[1]	30.34	64.37	-	-	-	9.04	20.54	24.04	79.23	-	-
Cavioidea	†*Neoreomys australis*[1]	30.86	55.79	-	-	-	15.05	27.53	19.81	49.36	-	-
	Cavia porcellus[1]	23.48	61.28	-	-	-	12.04	32.03	7.30	31.09	-	-
	Cavia aperea[3]	-	-	662	1,825	36.27	-	-	-	-	-	-
	Dolichotis patagonum[3]	-	-	2,892	6,938	41.68	-	-	-	-	-	-
	Hydrochoerus hydrochaeris[3]	-	-	6,237	15,877	39.28	-	-	-	-	-	-
	Hydrochoerus hydrochaeris[1]	62.95	62.56	-	-	-	13.46	14.4	30.32	48.16	-	-
	Kerodon (*Galea*) *spixii*[3]	-	-	623	1,701	36.63	-	-	-	-	-	-
	Kerodon rupestris[3]	-	-	749	2,258	33.17	-	-	-		-	-
	Dasyprocta sp.[1]	37.21	62.49	-	-	-	11.74	19.07	21.72	58.37	-	-
	Dasyprocta leporina[3]			2,222	6,021	36.90					-	-
	Dasyprocta variegata[3]	-	-	2,162	5,878	36.78	-	-	-	-	-	-
Chinchilloidea	*Dinomys branickii*[1]	45.01	64.98	-	-	-	11.64	16.43	30.65	68.10	-	-
	†*Neoepiblema acreensis*[1]	55.87	65.67	-	-	-	13.97	16.86	32.17	57.58	-	-
	Cuniculus paca[3]	-	-	3,308	9,093	36.38	-	-	-	-	-	-
	Chinchilla lanigera[1]	25.0	58.83	-	-	-	9.81	25.26	12.61	50.44	-	-
	Lagostomus maximus[1]	39.0	61.82	-	-	-	7.55	13.42	20.32	52.10	-	-
Paleogene non- caviomorph rodents	†*Ischyromys typus* (ROMV 1007)[2]	23.58	51.69	577.77	2,727.54	21.18	9.36	23.08	19.98	84.73	91.12	1.36
	†*Ischyromys typus* (AMNH 12252)[2]	20.06	47.51	572.78	3,105.22	18.45	9.02	22.83	-	-	-	-
	†*Ischyromys typus* (AMNH F:AM 144638)[2]	23.72	50.53	615.72	2,673.32	23.03	11.22	27.75	21.44	90.39	116.58	1.60
	†*Paramys copei*[4]	21.47	45.94	577.77	3,378.48	17.10	9.92	21.65	20.30	94.55	89.9	1.20
	†*Paramys delicatus*[4]	25.63	46.04	790.48	4,864.86	16.25	11.50	22.75	24.01	93.68	129.30	1.03
	†*Cedromus wilsoni*[5]	19.54	58.19	606.27	2,048.7	29.59	7.03	21.98	12.94	66.22	113.96	3.16
	†*Pseudotomus horribilis*[6]	32.11	48.58	1,103.54	5,842.8	18.89	12.63	23.23	29.31	91.28	196.90	1.30
	†*Pseudotomus oweni*[6]	23.0	54.52	1,087.42	4,744.38	22.92	10.30	19.91	23.83	103.61	77.00	0.64
	†*Pseudotomus petersoni*[6]	31.45	54.68	1,337.58	5,843.70	22.89	10.47	20.21	-	-	71.50	0.42
	†*Pseudotomus hians*[6]	32.34	49.87	1,123.12	4,878.63	23.02	12.22	25.58	29.64	91.65	142.40	1.04
	†*Reithroparamys delicatissimus*[6]	21.95	48.97	563.34	-	-	6.83	18.93	19.93	90.80	148.86	-
	†*Rapamys atramontis* (AMNH 128706)[6]	22.17	52.01	777.02	3,839.25	20.24	8.20	19.76	18.66	84.17	108.09	1.52
	†*Rapamys atramontis* (AMNH 128704)[6]	22.24	50.63	610.23	2,803.57	21.77	7.87	19.93	18.34	82.46	123.02	2.05

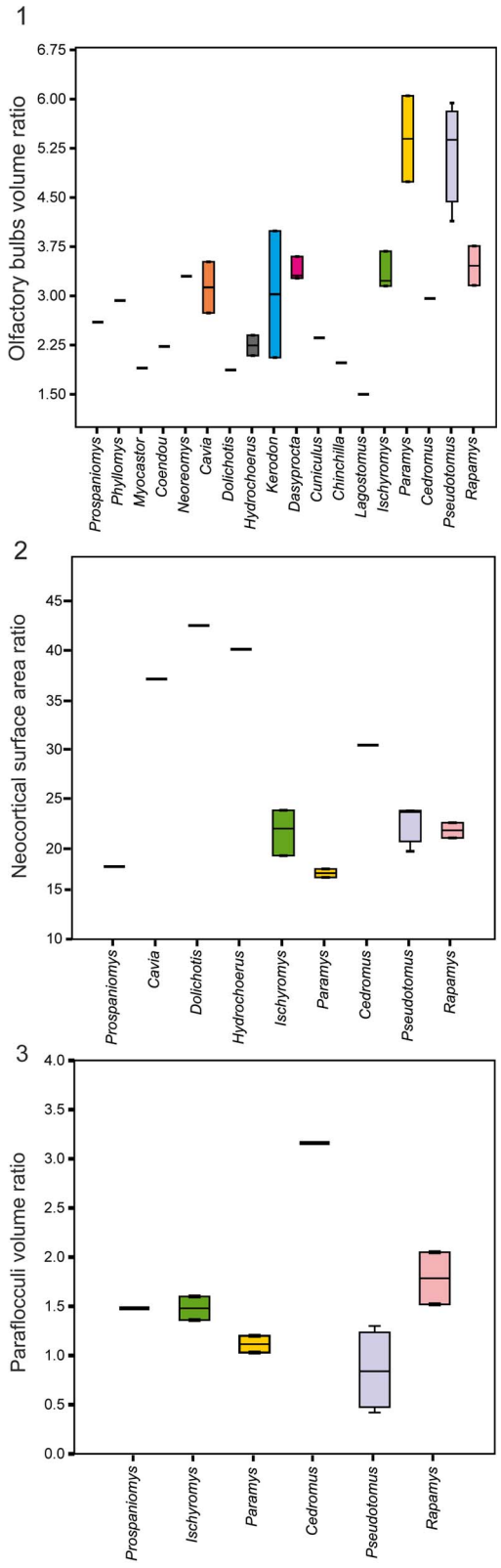

Figure 6. Boxplots showing the following comparisons: (**1**) olfactory bulbs volume with respect to total endocast volumes of *Prospaniomys*, the fossil cavioid *Neoreomys*, extant caviomorphs, and noncaviomorph rodents; (**2**) neocortical surface with respect to total endocast surfaces of *Prospaniomys*, extant caviomorphs, and Paleogene noncaviomorph rodents; (**3**) paraflocculi volume with respect to total volumes of endocasts of *Prospaniomys* and Paleogene noncaviomorph rodents.

endocranial volume (or endocranial mass, in g) and body mass. Endocranial mass was calculated following Bertrand and Silcox (2016) and was obtained by dividing the endocranial volume by 1.05. To calculate the body mass of *Prospaniomys*, we followed three steps: first, we made a bibliographic search of body masses of extant caviomorphs; then, we took several regression equations based on dental and cranial materials used in rodents (Legendre, 1986; Croft, 2000; Rinderknecht and Blanco, 2008; Freudenthal and Martín-Suárez, 2013; Bertrand et al., 2016a), and calculated the masses for those taxa; finally, we compared our new results with those found in the literature, and then we chose only those equations that better approximate the body mass of these extant taxa (Table 2, and Supplementary Data). In this regard, we dismissed those equations that over- or underestimated the body mass of *Prospaniomys* and the rodents used for comparison (i.e., Croft, 2000; Rinderknecht and Blanco, 2008). The body masses of the extinct and extant taxa used for comparisons were obtained from the literature (i.e., Dozo, 1997a; Bertrand and Silcox, 2016; Bertrand et al., 2016b, 2017, 2019; Ferreira et al., 2020, 2021).

We recalculated a few parameters not calculated in previous works to obtain the EQ of several caviomorphs. The EQ of *Dolicavia* was originally calculated based on endocranial volume (Dozo, 1997a), whereas in the adult specimen of *Hydrochoerus* Brisson, 1762, it was calculated following a different parameter (Ferreira et al., 2021). Thus, we recalculated endocranial masses and then both EQs, to obtain values that could be used for comparison in the present work (Table 2). The EQs of *Dolicavia*, *Cavia* Pallas, 1766, and *Dolichotis* Desmarest, 1819 were here calculated using the equations of Eisenberg (1981) and Pilleri et al., (1984), because Dozo (1997a) calculated the EQ using only the equation of Jerison (1973). Dozo (1997a) also used an equation based on parameters not considered in the present study and therefore was dismissed. Considering some taxa included by Ferreira et al., (2021), e.g., *Dolichotis patagonum* (Zimmermann, 1780), *Cavia*, species of *Dasyprocta* Illiger, 1811 and *Kerodon* Cuvier, 1823b, *Cuniculus paca* (Linnaeus, 1766), and *Galea musteloides* Meyen, 1833, we were not able to calculate EQs using the equations of Eisenberg (1981) and Pilleri et al., (1984) because the original information was not available.

Repositories and institutional abbreviations.—The specimen studied in this work is housed at the Vertebrate Paleontology Collection, Museo Argentino de Ciencias Naturales "Bernardino Rivadavia" (MACN-PV CH). Other cited repositories are AMNH, American Museum of Natural History, New York, USA; and ROMV, Royal Ontario Museum Vertebrate Paleontology, Toronto, Canada.

Description and comparisons

Prospaniomys priscus has a total endocast volume of 2,425.8 mm^3, similar to the small octodontoid *Phyllomys* Lund, 1839, and smaller than the remaining compared taxa (Table 1).

Olfactory bulbs.—In dorsal view, the olfactory bulbs are well-defined, slightly elongated, and oval (Fig. 4.1). This

https://doi.org/10.1017/jpa.2022.98 Published online by Cambridge University Press

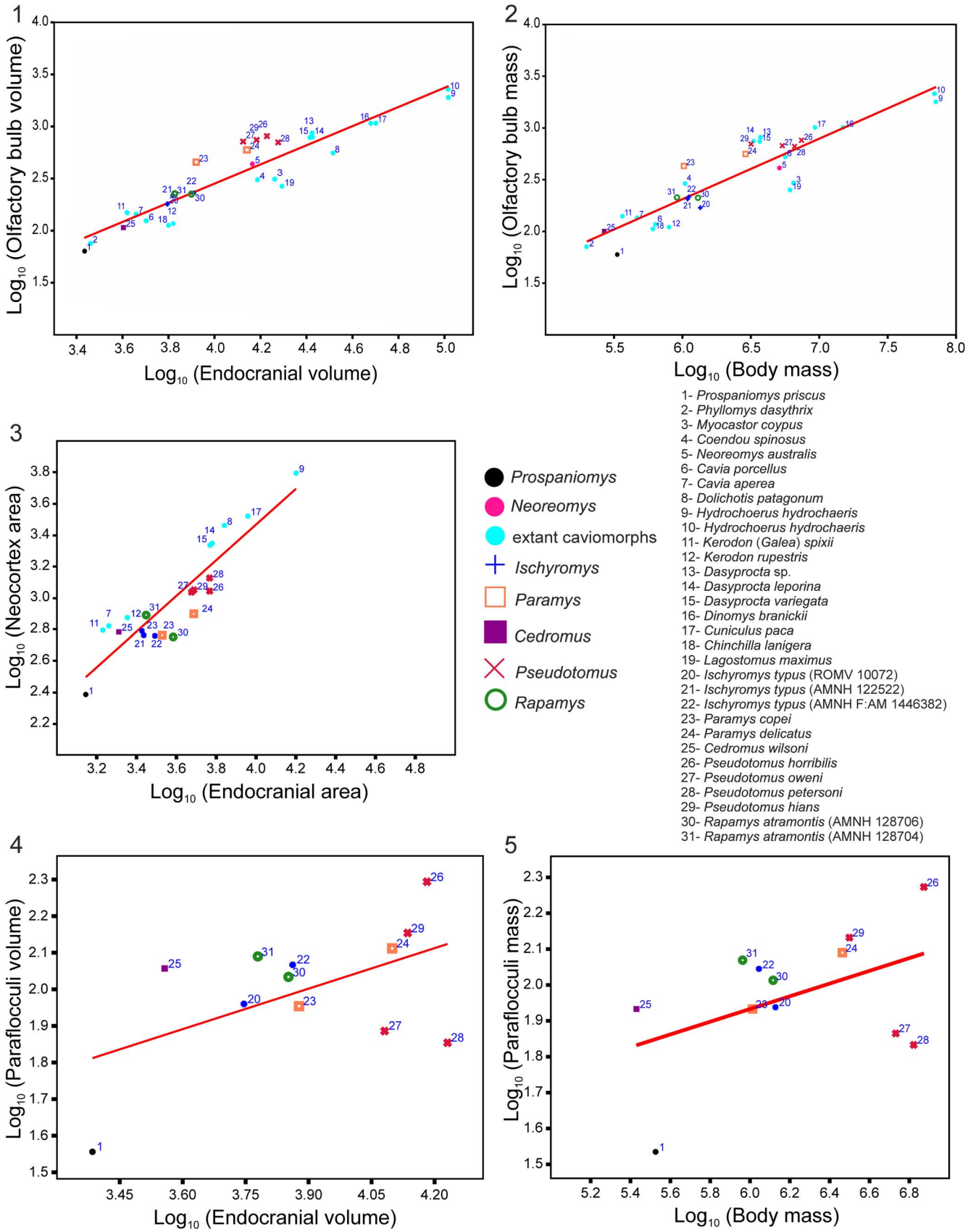

Figure 7. Regression plots of (**1**) $\log_{10}$ (olfactory bulbs volume, in mm^3) versus $\log_{10}$ (endocranial volume, in mm^3); (**2**) $\log_{10}$ (olfactory bulbs mass, in g) versus $\log_{10}$ (body mass, in g); (**3**) $\log_{10}$ (neocortical surface, in mm^2) versus $\log_{10}$ (endocranial surface, in mm^2); (**4**) $\log_{10}$ (paraflocculi volume, in mm^3) versus $\log_{10}$ (endocranial volume, in mm^3); (**5**) $\log_{10}$ (paraflocculi mass, in g) versus $\log_{10}$ (body mass, in g).

https://doi.org/10.1017/jpa.2022.98 Published online by Cambridge University Press

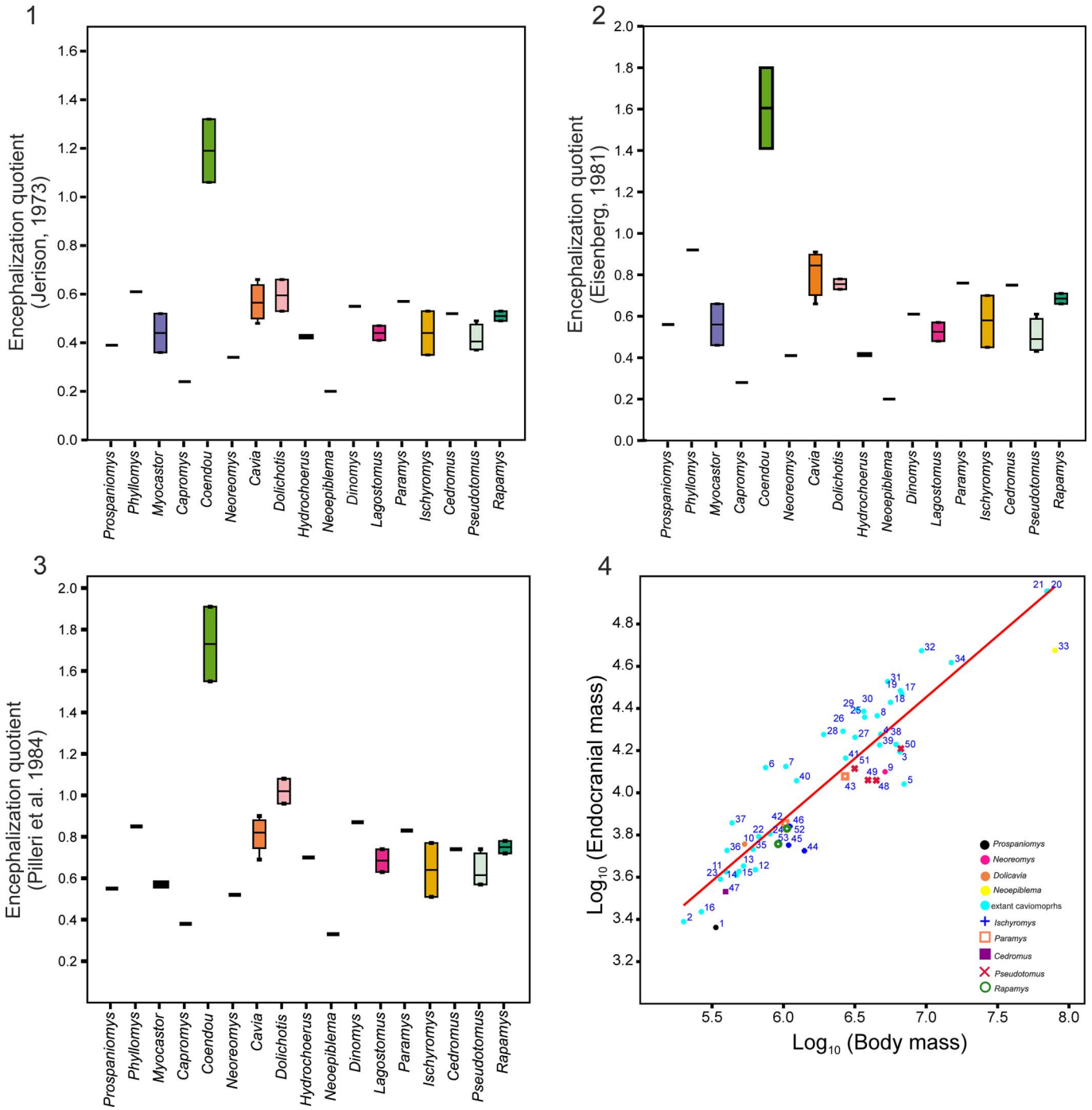

Figure 8. (**1–3**) Encephalization quotients of *Prospaniomys*, the fossil cavioid *Neoreomys*, the fossil chinchilloid *Neoepiblema*, extant caviomorphs (*Phyllomys*, *Myocastor*, *Capromys*, *Cavia*, *Dolichotis*, *Dinomys*, and *Lagostomus*), and fossil noncaviomorph rodents (*Paramys*, *Ischyromys*, *Cedromus*, *Pseudotomus*, and *Rapamys*): (**1**) based on Jerison's (1973) equation; (**2**) based on Eisenberg's (1981) equation; (**3**) based on Pilleri et al.'s (1984) equation; (**4**) regression plot of $\log_{10}$ (endocranial mass, in g) versus $\log_{10}$ (body mass, in g). 1 = *Prospaniomys priscus*; 2 = *Phyllomys dasythrix* Hensel, 1872; 3 and 4 = *Myocastor coypus* Kerr, 1792; 5 = *Capromys pilorides* (Say, 1822); 6 and 7 = *Coendou spinosus* Cuvier, 1823a; 8 = *Erethizon dorsatum* (Linnaeus, 1758); 9 = *Neoreomys australis* Ameghino, 1887; 10 = *Dolicavia minuscula* Ameghino, 1908; 11 = *Cavia* sp.; 12 and 13 = *Cavia porcellus* Trouessart, 1897; 14 and 15 = *Cavia aperea* Erxleben, 1777; 16 = *Galea musteloides*; 17 = *Dolichotis* sp.; 18 and 19 = *Dolichotis patagonum*; 20 and 21= *Hydrochoerus hydrochaeris* (Linnaeus, 1766); 22 and 23 = *Kerodon spixii* (Trouessart, 1897); 24 = *Kerodon rupestris* (Wied-Neuwied, 1820); 25 = *Dasyprocta* sp.; 26 = *Dasyprocta aguti* (Linnaeus, 1766) sensu Bertrand and Silcox (2016), junior synonym of Dasyprocta leporina and D. croconota sensu Patton and Emmons (2015); 27 = *Dasyprocta punctata* Gray, 1842; 28 = *Dasyprocta mexicana* (Saussure, 1860); 29 = *Dasyprocta leporina* (Linnaeus, 1758); 30 = *Dasyprocta variegata* Tschudi, 1845; 32 = *Cuniculus paca*; 33 = *Neoepiblema acreensis* Bocquentin, Filho, and Negri, 1990; 34 = *Dinomys branickii* Peters, 1873; 35 and 36 = *Chinchilla lanigera* Bennett, 1829; 37 = *Chinchilla brevicaudata* Waterhouse, 1848; 38 and 39 = *Lagostomus maximus*; 40 and 41 = *Lagidium viscacia* (Molina, 1782); 42 = *Paramys copei* Loomis, 1907; 43 = *Paramys delicatus* Leidy, 1871; 44 = *Ischyromys typus* (ROMV 10072); 45 = *Ischyromys typus* (AMNH 122522); 46 = *Ischyromys typus* (AMNH F:AM 1446382); 47 = *Cedromus wilsoni*; 48 = *Pseudotomus horribilis* Wood, 1962; 49 = *Pseudotomus oweni*; 50 = *Pseudotomus petersoni* Matthew, 1910; 51 = *Pseudotomus hians*; 52 = *Rapamys atramontis* Wahlert, Korth, and McKenna, 2006 (AMNH 128706); 53 = *Rapamys atramontis* (AMNH 128704).

https://doi.org/10.1017/jpa.2022.98 Published online by Cambridge University Press

Table 2. Brain mass, body mass, and encephalization quotients (EQs). 1 = Ferreira et al. (2020); 2 = Dozo (1997b); 3 = Bertrand and Silcox (2016): the mean value (x̄) was calculated in those species represented by several specimens; 4 = Ferreira et al. (2021); 5 = Bertrand et al. (2016); 6 = Bertrand et al. (2017); 7 = Bertrand et al. (2019); * = calculated in this work; † = fossil species.

				EQ		
	Taxon	Brain mass (g)	Body mass (g)	Jerison (1973)	Eisenberg (1981)	Pilleri et al. (1984)
Pan-Octodontoidea	†*Prospaniomys priscus*	2.3	336.1	0.39	0.56	0.55
Octodontoidea	*Phyllomys dasythrix*[1]	2.45	200	0.61	0.92	0.85
	Myocastor coypus[1]	15.65	6,530	0.36	0.46	0.56
	Myocastor coypus[3] (x̄)	18.95	4,795.76	0.52	0.66	0.58
	Capromys pilorides[3]	11	7,000	0.24	0.28	0.38
Erethizontoidea	*Coendou spinosus*[1]	13.17	750	1.32	1.8	1.91
	Coendou spinosus[1]	13.33	1,040	1.06	1.41	1.55
	Erethizon dorsatum[3] (x̄)	23.19	4,542.27	0.79	0.95	1.20
Cavioidea	†*Neoreomys australis*[1]	12.58	5,150	0.34	0.41	0.52
	†*Dolicavia minuscula*[2]	5.71*	534.5	0.70*	0.98*	1.01*
	Cavia[2]	4.22	396.6	0.66*	0.91*	0.90*
	Cavia porcellus[1]	4.32	637	0.48	0.66	0.69
	Cavia porcellus[3] (x̄)	4.50	525.47	0.56	0.86	0.86
	Cavia aperea[3] (x̄)	4.07	468.75	0.57	0.83	0.82
	Cavia aperea[4]	4.24	489	-	-	0.80
	Galea musteloides[4]	2.73	266	-	-	1.26
	Dolichotis[2]	29.4	6,746	0.66	0.78*	1.02*
	Dolichotis patagonum[3] (x̄)	26.83	5,625.71	0.53	0.73	0.96
	Dolichotis patagonum[4]	30.47	6,585	-	-	1.08
	Hydrochoerus hydrochaeris[4]	90.5*	71,482	0.42	0.41	0.7
	Hydrochoerus hydrochaeris[1]	90.24	69,950	0.43	0.42	0.7
	Kerodon spixii[3]	6.20	672	0.66	0.91	0.95
	Kerodon (*Galea*) *spixii*[4]	3.895	362	-	-	0.89
	Kerodon rupestris[4]	6.40	804	-	-	0.88
	Dasyprocta sp.[1]	22.84	3,700	0.77	0.95	1.17
	Dasyprocta agouti[3] (x̄)	19.58	2,615.54	0.84	1.06	1.27
	Dasyprocta puntacta[3]	18.34	3,172	0.69	0.85	1.04
	Dasyprocta mexicanus[3] (x̄)	18.9	1,913.5	1.01	1.3	1.48
	Dasyprocta leporina[4]	24.82	3,287	-	-	1.38
	Dasyprocta variegata[4]	24.342	3,654	-	-	1.26
Chinchilloidea	*Cuniculus paca*[3] (x̄)	33.67	5,373	0.92	1.1	1.04
	Cuniculus paca[4]	47.15	9,275	-	-	1.34
	†*Neoepiblema acreensis*[1]	47.31	79,750	0.20	0.20	0.33
	Dinomys branickii[1]	41.43	15,000	0.55	0.61	0.87
	Chinchilla lanigera[1]	5.40	612	0.61	0.85	0.88
	Chinchilla lanigera[3] (x̄)	5.33	402.75	0.80	1.14	1.14
	Chinchilla brevicaudata[3] (x̄)	7.2	437	1.03	1.46	1.47
	Lagostomus maximus[1]	16.96	6,150	0.41	0.48	0.63
	Lagostomus maximus[3] (x̄)	16.85	4,721.12	0.47	0.57	0.74
	Lagostomus peruanum[3] (x̄)	11.41	1,237.05	0.83	1.09	1.22
	Lagidium viscacia[3] (x̄)	14.6	2,726.75	0.63	0.78	0.94
Paleogene noncaviomorph rodents	†*Paramys copei*[5]	7.17	1,029.89	0.57	0.76	0.83
	†*Paramys delicatus*[5]	11.97	2,704.83	0.50	0.62	0.75
	†*Ischyromys typus*[3]	5.31	1,401.8	0.35	0.45	0.51
	†*Ischyromys typus*[3]	5.65	1,086.42	0.44	0.58	0.64
	†*Ischyromys typus*[3]	6.93	1,109.01	0.53	0.70	0.77
	†*Cedromus wilsoni*[6]	3.4	393.49	0.52	0.75	0.74
	†*Pseudotomus horribilis*[7]	11.46	4,472.67	0.43	0.52	0.66
	†*Pseudotomus oweni*[7]	11.49	3,911.71	0.38	0.46	0.57
	†*Pseudotomus petersoni*[7]	16.20	6,644.56	0.37	0.43	0.57
	†*Pseudotomus hians*[7]	13.03	3,153.50	0.49	0.61	0.74
	†*Reithroparamys delicatissimus*[7]	-	843.33	-	-	-
	†*Rapamys atramontis* (AMNH 128706)[7]	6.77	1,057.82	0.53	0.71	0.78
	†*Rapamys atramontis* (AMNH 128704)[7]	5.72	918.73	0.49	0.66	0.72

morphology is similar to those of *Neoepiblema*, *Phyllomys*, and *Chinchilla* Bennet, 1829, and differs from the olfactory bulbs of *Hydrochoerus*, which have an irregular shape. Their anterior extension cannot be determined accurately because the cribriform plate is not well preserved, but they extend anteriorly over the posterior margin of the M1, as in *Rapamys* and *Ischyromys* (Bertrand and Silcox, 2016; Bertrand et al., 2019). In ventral view, the olfactory tracts, which connect the olfactory bulbs with the piriform lobes, were clearly observed (Fig. 4.2).

The olfactory bulbs represent ~2.6% of the total endocast volume, 14.1% of the total length of the endocast, and 30.8% of the total width (Table 1). These values are considerably lower compared with the Paleogene noncaviomorph rodents, especially *Pseudotomus* and *Paramys* (Fig. 6.1; Table 1). In addition, *Prospaniomys* also has smaller values than the late early Miocene *Neoreomys* Ameghino, 1887, the only fossil caviomorph with available olfactory bulb data (Fig. 6.1; Table 1). Compared with the living pan-octodontoids, *Prospaniomys* has a relatively low olfactory bulb volume percentage with

https://doi.org/10.1017/jpa.2022.98 Published online by Cambridge University Press

respect to the arboreal *Phyllomys*, although higher than the aquatic *Myocastor* Kerr, 1792 (Fig. 6.1; Table 1). Comparing the olfactory bulb volume with respect to the endocranial volume, *Prospaniomys* has the smallest olfactory bulbs of the sample, close to those of *Phyllomys*, whereas *Hydrochoerus* is the taxon that presents the largest olfactory bulbs (but also the highest endocranial volume) (Fig. 7.1). In this regard, we also observed that most extant caviomorphs have olfactory bulbs smaller than expected for their endocranial volume. On the other hand, the Eocene–Oligocene fossil noncaviomorphs show olfactory bulb volume larger than expected for their endocranial volume (Bertrand et al., 2019; Fig. 7.1), except for *Cedromus* Wilson, 1949, the most ancient squirrel, which is below the regression line and close to *Prospaniomys* and *Phyllomys*. Regarding the mass of the olfactory bulbs, *Prospaniomys* also has one of the smallest values with respect to its body mass (Fig. 7.2). In addition, *Phyllomys*, *Myocastor*, *Cavia*, *Kerodon*, *Chinchilla*, and *Lagostomus* Brookes, 1829 also have olfactory bulb masses below those expected for their body masses, whereas the rest of the extant caviomorphs plotted above the regression line (Fig. 7.2). The noncaviomorphs *Ischyromys*, *Rapamys*, and *Cedromus* fell below the regression line, whereas *Pseudotomus* and *Paramys* were above, but close to the regression line (Fig. 7.2), as was expressed by Bertrand et al., (2019).

Cerebrum and mesencephalon.—The circular fissure that separates the olfactory bulbs from the frontal lobes of the cerebrum is dorsally and laterally narrow and well-marked, unlike that of *Hydrochoerus* in which it is not evident. Thus, the cerebrum is close to the olfactory bulbs, as in most rodents but unlike in *Paramys*, one specimen of *Ischyromys* (ROMV 1007; Bertrand and Silcox, 2006), and the living *Hydrochoerus* and *Lagostomus* in which both structures are farther placed. In lateral view, the endocast of *Prospaniomys* has its components (i.e., olfactory bulbs, cerebrum, and cerebellum) anteroposteriorly aligned (Fig. 4.3), as in Paleogene noncaviomorph rodents and one fossil caviomorph (i.e., Cephalomyidae gen. indet. sp. indet.; Dozo, 1997b), and unlike most known caviomorphs (Madozzo-Jaén, 2019; Ferreira et al., 2020).

In dorsal view, the cerebrum is slightly triangular (Fig. 4.1), unlike in *Phyllomys*, *Myocastor*, *Dinomys* Peters, 1873, erethizontids, and Paleogene noncaviomorph rodents that have clearly rounded lateral cerebral margins (Fig. 5). The cerebral hemispheres are anteriorly narrow with the frontal lobes not greatly laterally expanded, unlike in *Phyllomys*, *Coendou* Lacépède, 1799, *Hypsosteiromys*, *Neoepiblema*, and *Dinomys* (Dozo, 1997b; Dozo et al., 2004; Ferreira et al., 2020; Fig. 5). Caudally, each cerebral hemisphere becomes wider, forming lateral temporal lobes (sensu Dozo, 1997a, b), and then narrows abruptly in their posteriormost third, delimiting a morphology similar to that observed in Cephalomyidae gen. indet. sp. indet., *Hydrochoerus*, *Dolicavia*, *Cavia*, *Prodolichotis* Kraglievich, 1932, *Dolichotis*, *Lagostomus*, *Galea* Meyen, 1833, and *Chinchilla* (Madozzo-Jaén, 2019; Ferreira et al., 2020, 2021; Fig. 5). However, *Prospaniomys* differs from *Dolicavia*, *Cavia*, *Prodolichotis*, *Dolichotis*, *Galea*, *Kerodon*, and *Hydrochoerus* in having continuous lateral margins of the cerebral hemispheres, whereas in the above-mentioned cavioids, a conspicuous sulcus (= suprasylvian sulcus; see below) separates the anterior part of the cerebral hemispheres from the posterior lateral expansions (Madozzo-Jaén, 2019; Ferreira et al., 2020, 2021; Fig. 5). In its posteromedial region, each hemisphere becomes more separated from the other by bifurcation of the longitudinal fissure (see below; Fig. 4.1), as in Cephalomyidae gen. indet. sp. indet. (Fig. 5.9). In lateral view, the cerebrum has a slightly rounded dorsal surface (Fig. 4.3). The frontal lobes do not dorsally cover the olfactory bulbs, as in most caviomorphs (Dozo, 1997b; Dozo et al., 2004; Madozzo-Jaén, 2019; Ferreira et al., 2020, 2021) and Paleogene noncaviomorph rodents (Bertrand and Silcox, 2016; Bertrand et al., 2017, 2018, 2019; Fig. 5). Posteriorly, the cerebral hemispheres also do not dorsally cover part of the mesencephalon or the cerebellum, as in the most ancient rodents considered here (Fig. 5.2–5.6), and unlike in *Neoepiblema* and several living caviomorphs (Madozzo-Jaén, 2019; Ferreira et al., 2020, 2021; Fig. 5.7–5.8, 5.10–5.11).

Prospaniomys presents a lissencephalic cerebrum with a few shallow sulci (Fig. 4), as in some caviomorphs and most noncaviomorph rodents (Fig. 5). These sulci are much shallower than those observed in *Phyllomys*, *Myocastor*, *Dolicavia*, *Prodolichotis*, *Cavia*, *Hydrochoerus*, *Chinchilla*, *Galea*, *Kerodon*, *Lagostomus*, and *Dinomys* (Dozo, 1997a; Campos and Welker, 1976; Ferreira et al., 2020, 2021). The longitudinal fissure is anteroposteriorly oriented in the sagittal plane between the cerebral hemispheres and is conspicuous over its entire length. Its anterior half is slightly broader than its posterior half and bears a thin longitudinal ridge that corresponds to the mark of the suture between the frontal bones (Fig. 4.1). The longitudinal fissure continues posteriorly to meet the transverse fissure. It runs laterally and then down to the ventral surface of the cerebrum, near the posterior margin of the sphenorbital fissure. Other shallower depressions of the cerebrum endocast are interpreted as sulci. For example, in lateral view, a shallow sulcus was observed at the anteroposterior midpoint of the cerebral hemispheres. Its anterior portion is dorsoventrally oriented, and it then runs upward and posteriorly parallel to the longitudinal fissure (Fig. 4.3). This latter sulcus could correspond to the suprasylvian sulcus (= Sylvian fissure sensu Ferreira et al., 2021), which separates the frontal lobe from the temporal lobe of the cerebrum (Dozo, 1997a; Ferreira et al., 2021). Medial to this sulcus and between the longitudinal fissure, another short sulcus is located in the caudal region of the cerebrum (Fig. 4.1), which could correspond to the lateral sulcus (= lateral sulcus a sensu Ferreira et al., 2020, 2021).

In mammals, the rhinal sulcus is a neuroanatomic landmark of relevance that delimits the neocortex of the cerebral cortex from the paleocortex and allows one to determine the degree of cerebralization of the taxon under study (Jerison, 2012). In *Prospaniomys*, the rhinal sulcus is conspicuous. Its anterior portion was observed lateral to the olfactory tract (Fig. 4.2), whereas posteriorly it is lateral to the piriform lobe. In ventral view, the piriform lobe is round, whereas in lateral view it is dome-shaped (Fig. 4.3). Anteriorly, it is delimited by part of the shallow suprasylvian sulcus, laterally by the rhinal sulcus, medially by the sphenorbital fissure, and posteriorly by the middle lacerate foramen.

On the endocast surface, a few thin impressions of bone sutures were observed. The most conspicuous sutures correspond to the bones of the cranial roof: the above-mentioned mark of the

https://doi.org/10.1017/jpa.2022.98 Published online by Cambridge University Press

frontals suture and the mark of the suture between the frontals and parietals, which is transverse to the former (Fig. 4.1). In lateral view, the mark of the sutures between the frontal and squamosal and between the squamosal and parietal bones were observed (Fig. 4.3). The suture between the frontals and orbitosphenoid was observed in the anteroventral face of the endocast (Fig. 4.3). Other well-marked bone sutures between the auditory bulla with the squamosal and the alisphenoid are evident.

In dorsal view and posterior to the cerebral hemispheres, a plane and triangular area interpreted as the tectum of the mesencephalon was observed (Fig. 4.1). A similar morphology is present in Cephalomyidae gen. indet. sp. indet. and other Paleogene noncaviomorph fossil rodents (Dechaseaux, 1958; Bertrand and Silcox, 2016; Bertrand et al., 2017, 2018, 2019; Fig. 5.2–5.6, 5.9). The caudal colliculi (= inferior colliculi of Bertrand and Silcox, 2016), which are part of the auditory complex (Liem et al., 2001; Evans and de Lahunta, 2013), are not evident in this specimen of *Prospaniomys*, as in several Paleogene noncaviomorph rodents (e.g., *Paramys* (Fig. 5.4), some specimens of *Ischyromys* (ROMV 1007, AMNH 12252; Bertrand et al., 2016b), and the ancestral squirrel *Cedromus*; (Fig. 5.6), whereas they are visible in one specimen of *Ischryromys* (AMNH F:AM 144638; Fig. 5.4) and in *Reithroparamys* (Fig. 5.3). However, this could be due to the poor preservation of this region. This area is not described for any other caviomorph.

The ratio of the cerebral maximum length with respect to the total endocranial length in *Prospaniomys* is higher than in fossil noncaviomorphs, although similar to caviomorphs, especially the living *Phyllomys* and *Chinchilla* (Table 1). The neocortical surface area ratio of *Prospaniomys* is one of the lowest of the sample, together with those values calculated for *Paramys* (Fig. 6.2; Table 1). The regression analysis of the neocortical area with respect to the total endocranial area demonstrates that the surface area of *Prospaniomys* is the smallest of the sample and also is smaller than would be expected for its endocranial area (Fig. 7.3). The surface area of the neocortex in extant caviomorphs is higher than that expected for their endocranial surface area (Fig. 7.3), whereas fossil noncaviomorphs fall below the regression line, except for *Cedromus* and one specimen of *Rapamys* (AMNH 128704), which are close to the regression line (Fig. 7.3).

Cerebellum.—As mentioned above, in *Prospaniomys*, the cerebellum is not dorsally covered by the cerebral hemispheres, and therefore its dorsal surface is entirely visible. We recognized the central, prominent vermis and the lateral cerebellar hemispheres (Fig. 4.1). Both structures are separated by shallow paramedian fissures. This morphology is similar to those observed in Cephalomyidae gen. indet. sp. indet. and *Phyllomys*, but is different from those of *Myocastor*, *Neoepiblema*, and *Coendou* (Fig. 5.9–5.11). On the dorsal surface of each cerebellar hemisphere, at its midpoint, is a shallow transverse sulcus (Fig. 4.1). It is limited medially by the paramedian fissure and laterally by the cast of a small vessel. The vermis does not present any sulcus on its surface.

The percentage of the anteroposterior length of the cerebellum with respect to the total endocranial length is almost 24.9%, similar to that of living *Chinchilla*, smaller than in *Cavia* and *Neoreomys*, and clearly higher than those of the rest of the caviomorphs studied by Ferreira et al. (2020; Table 1). With respect to the Paleogene noncaviomorph rodents, the length of the cerebellum is shorter than that of *Pseudotomus hians* Cope, 1872, falls within the values for *Ischyromys*, and is longer than in the remaining noncaviomorph fossils (Table 1). The cerebellum is laterally narrower than the cerebrum (the paraflocculi were not taken into consideration), as in most caviomorphs (Fig. 5.1, 5.7–5.12). The percentage of the width of the cerebellum with respect to the cerebrum is 69.2%, a higher value than in most caviomorphs (with the exception of *Phyllomys* and *Coendou*), but lower than in most Paleogene noncaviomorphs (Table 1). That means that *Prospaniomys* is the caviomorph with the greatest length and width proportions of the cerebellum (Fig. 5).

The paraflocculi are better observed in lateral view (Fig. 4.3). They are well-developed, unlike in *Neoepiblema* (Ferreira et al., 2020), are globular, and are located lateroventral to the cerebellar hemispheres (Fig. 4.3). The percentage of the paraflocculi volume with respect to the volume of the total endocast is 1.48%, a higher value than in *Paramys*, *Pseudotomus*, and most specimens of *Ischyromys*. Only *Rapamys*, *Cedromus*, and one specimen of *Ischyromys* had higher values (Fig. 6.3; Table 1). On the contrary, when the volume and the mass of the paraflocculi are plotted against the total endocranial volume and the body mass, respectively, *Prospaniomys* has the lowest values and each falls well below the regression line (Fig. 7.4, 7.5). However, in both cases, the analysis shields nonsignificant values because the available information is scarce. Unfortunately, there are no parafloccular quantitative data for other caviomorph rodents. *Prospaniomys* follows the anatomical rule expressed by Ferreira et al. (2020), i.e., in those caviomorphs with evident paraflocculi, the cerebral hemispheres do not dorsally cover the cerebellum.

Brainstem and cranial nerves.—Different cranial foramina were identified and used to reconstruct the paths of the cranial nerves and vascular system.

In ventral and lateral views, and posterior to the olfactory bulbs, nerve II (= optic tract) was observed, whereas the optic chiasma was not evident (Figs. 4.2, 4.3). The former passes through the large optic foramen that pierces the orbitosphenoid bone (Fig. 9). Posteriorly and in ventral view, we observed an outgoing structure for the passage of veins and nerves III (oculomotor), IV (trochlear), V_1 (deep ophthalmic ramus of the trigeminus nerve), V_2 (maxillary ramus of the trigeminus nerve), and VI (abducens) (Fig. 4.2). Unfortunately, the detailed courses of these cranial nerves could not be traced in the virtual 3D endocast of *Prospaniomys* because of preservation. Therefore, we could not determine if the V_2 runs together with the remaining above-mentioned nerves and vessels through the sphenorbital fissure, or if it has a distinct but confluent passageway. In this sense, Wahlert (1974) described that the sphenorbital fissure and the foramen rotundum are confluent in most rodents, a condition also present in other mammals, and therefore considered ancestral for Eutheria (Novacek, 1986). The masseteric and buccinator divisions of nerve V_3 are fused and pass through the fused masticatory and buccinator foramina (Figs. 4.2, 9), unlike in *Paramys*, *Pseudotomus*, and *Reithroparamys*, in which both branches and foramina are separated (Bertrand et al., 2019).

https://doi.org/10.1017/jpa.2022.98 Published online by Cambridge University Press

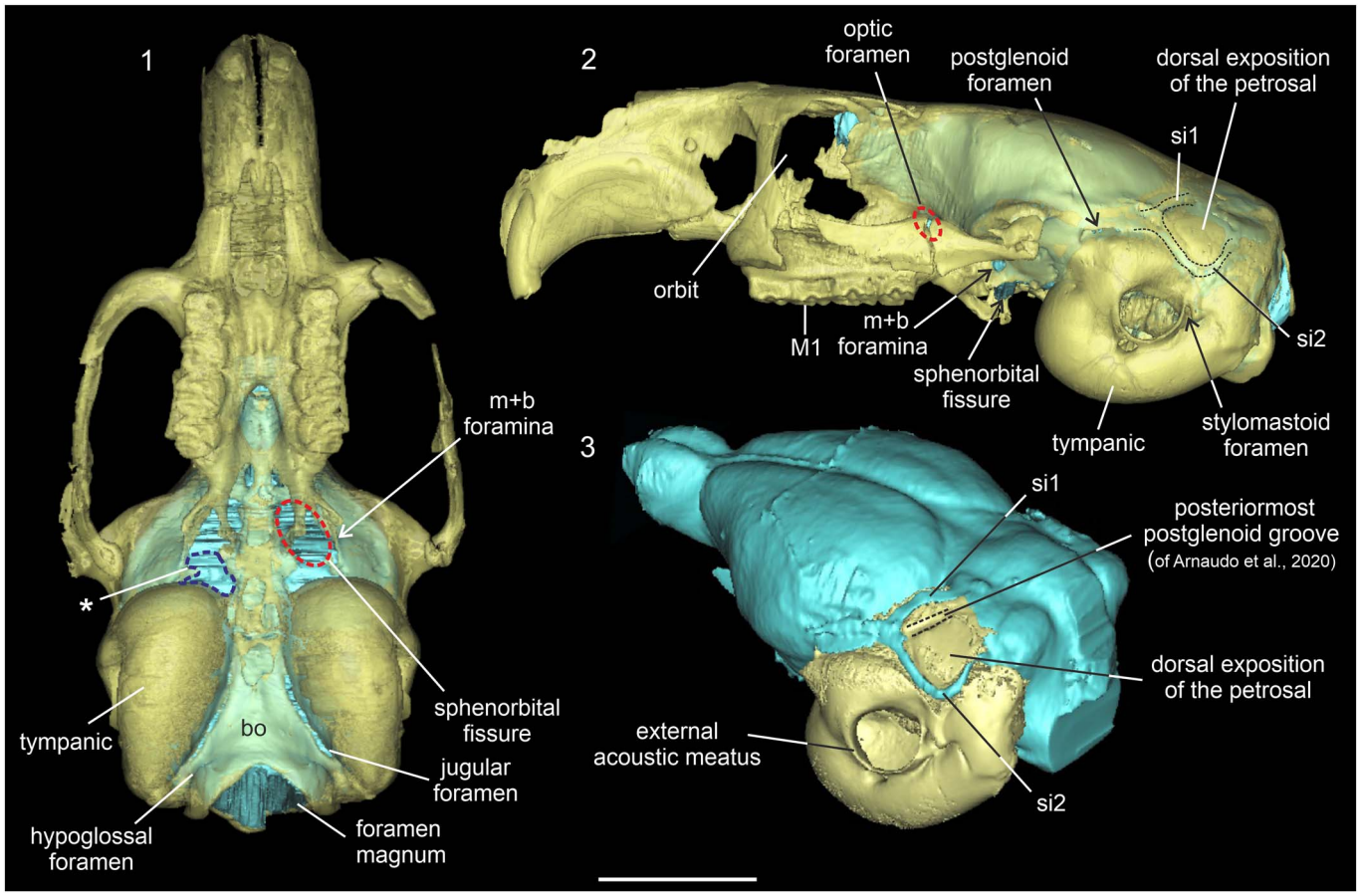

Figure 9. Translucent cranium of *Prospaniomys priscus* (MACN-PV CH1913) in (**1**) ventral and (**2**) left lateral views with the virtual cranial endocast (light blue) inside; (**3**) posterolateral view of the cranial endocast (light blue) and auditory bones (yellow). bo = basioccipital; M1 = upper first molar; m+b = masticatory + buccinator foramina; si1 = sinus 1; si2 = sinus 2; * = area that corresponds to broken foramen ovale and middle lacerate foramen (delimited by dashed blue line). The dashed red circles indicate different foramina: m+b foramina and the optic foramen that opens behind the zygomatic arc. Scale bar = 10 mm.

This opening was observed posterolateral to the sphenorbital fissure (Figs. 4.2, 9). Posteriorly, there is a medial portion of the endocast that could not be clearly reconstructed (Fig. 4.2, area delimited by blue dash lines) because the cranium is damaged. However, on the left side, a short extension interpreted as the mandibular ramus of nerve V_3 was observed (Fig. 4.2). This branch passes through the foramen ovale and should be laterally located at the posterior border of the sphenorbital fissure (Figs. 4.2, 9.1). However, owing to breakage, it was not possible to observe whether this foramen is isolated or fused to the middle lacerate foramen (Hill, 1935; Wahlert, 1985).

Nerves VII (facial) and VIII (vestibulocochlear) pass through the internal acoustic meatus, which opens on the cerebellar surface of the petrosal bone, anteroventral to the paraflocculus (Fig. 4.3), as in the Paleogene noncaviomorph rodents (Bertrand et al., 2019). Nerve VII runs into a complete bony facial canal and exits the cranium through the stylomastoid foramen (Fig. 9.2). Caviomorph rodents have lost the stapedial artery, and therefore the facial canal is not interrupted by the passage of this vessel, unlike in several North American or European rodents in which the stapedial artery enters the facial canal and exits the auditory bulla through several possible routes (Lavocat and Parent, 1985; Argyle and Mason, 2008; Mason, 2015). Nerve VIII presents a vestibular branch that innervates the vestibule and the ampulla of the semicircular canals of the inner ear, and the cochlear branch that runs through the modiolus (see Arnaudo et al., 2020, for further details).

Nerves IX (glossopharyngeal), X (vagus), and XI (accessory), as well as the internal jugular vein, pass through the jugular foramen, medial to the tympanic bullae (Figs. 4.2, 9.1), as is usual for Rodentia. Nerve XII (hypoglossal) passes through the hypoglossal foramen (Figs. 4.2, 9.1), located posterior to the jugular foramen. This is formed by a single, thin opening, as in most Paleogene noncaviomorph rodents and most caviomorph rodents (Bertrand et al., 2016a, 2019), but unlike the condition in the ancestral *Pseudotomus oweni* Marsh, 1872 and *Ischyromys typus* Leidy, 1856, which have two foramina (Bertrand and Silcox, 2016; Bertrand et al., 2019).

The hypophyseal fossa for the pituitary gland (Liem et al., 2001; Evans and de Lahunta, 2013) was not observed in the virtual 3D endocast. This could be related to the quality of preservation of the fossil in this region.

Blood vessels.—Several vascular casts could be reconstructed. However, because the presence/absence and disposition of blood vessels are highly variable in rodents (Bugge, 1985; Wahlert, 1985; Wible, 1987), in opposition to the cranial nerves, and the anatomical information is very scarce for

https://doi.org/10.1017/jpa.2022.98 Published online by Cambridge University Press

caviomorphs, several aspects are tentatively described and would be confirmed with future dissections. In dorsal view, the transverse sinus runs along the transverse fissure and continues posterolaterally with another sinus (Fig. 9.3). Then, it runs anterolaterally bordering the anterodorsal margin of the dorsal exposition of the petrosal and ends in the postglenoid foramen (Fig. 4.1, 4.3, sinus 1). This sinus runs through the anteriormost of the two grooves described as the postglenoid grooves by Arnaudo et al. (2020; Fig. 9.3). In our reconstructions, it was not possible to observe the structure or vessel that runs over the posteriormost postglenoid groove of Arnaudo et al. (2020; Fig. 9.3). The postglenoid foramen transmits a large vein that drains most of the cranial cavity and the encephalon (Hill, 1935; Wahlert, 1985; Wible and Shelley, 2020; Fig. 4.3). This vein was recognized as the postglenoid vein when it exits the cranium (Wible and Shelley, 2020).

Bordering the ventral margin of the dorsal exposition of the petrosal, we identified another sinus (Figs. 4.1, 4.3, 9.3, sinus 2). This sinus is longer, thinner, and more sinusoid than sinus 1. Sinus 2 extends anteriorly from a common area with sinus 1 next to the postglenoid foramen to the posteroventral margin of each lateral cerebellar hemisphere (Figs. 4.3, 9.3). This sinus runs over the anterior part of the postglenoid groove, the anterior branch of the posterior vertical channel, and the lateral groove of Arnaudo et al. (2020; fig. 4E). Posteriorly, sinus 2 continues with a sinus located in the junction of the petrosal with the exoccipital, which ends in the jugular foramen. This was recognized as the sigmoid sinus by Arnaudo et al. (2020). Anteriorly to the jugular foramen is a short, thin sinus that could correspond to the inferior petrosal sinus (Fig. 4.2) like the general morphology described for other rodents (Bertrand and Silcox, 2016).

In lateral view, a vascular impression is located over the suprasylvian sulcus and its posterior limit is the postglenoid foramen (Fig. 4.3, a). Two other blood vessel casts were identified in the posteroventral view of the endocast. The anteriormost, observed only on the right side, is oblique and runs from a point posterior to the postglenoid foramen and the middle lacerate foramen (Fig. 4.3, b). The second vessel is more notable, is L-shaped, and extends between the junction point of sinuses 1 and 2 and the middle lacerate foramen (Fig. 4.3, c). Dorsally, this latter vessel passes through a small foramen in the anterodorsal region of the cerebellar face of the petrosal (Fig. 4.2, asterisk). Ventrally, it leaves a mark on the dorsal surface of the petrosal (see Arnaudo et al., 2020). Some other casts of small vessels were observed in the dorsal region of the cerebral hemispheres. The orbitotemporal canal could not be reconstructed.

Living caviomorphs (also African hystricognaths) lack the internal carotid system; the brain is supplied by the vertebral-basilar arterial system, assisted by the external carotid (Bugge, 1985). The only exception to this general pattern are living erethizontids, in which the internal carotid is present (Bugge, 1985). In this work, we could not find signs of a carotid canal, which means that at least pan-octodontoids lost this vessel by the early Miocene. However, this interpretation needs to be confirmed by future dissections.

Brain size and encephalization quotient (EQ).—The specimen of *Prospaniomys* studied here is an adult specimen based on cheek-tooth wear and closure of the cranial sutures. To estimate its EQ, we first calculated the volume of the encephalon (2,425.8 mm^3) and the body mass (336.1 g). The EQs of all caviomorph and noncaviomorph rodents used in this work are listed in Table 2. *Prospaniomys* has a slightly higher EQ (considering the three equations) than the late early Miocene *Neoreomys*, and a clearly higher EQ than the giant late Miocene *Neoepiblema*, but a lower value than the late Pliocene *Dolicavia* (Fig. 8.1–8.3; Table 2). The EQ of the contemporaneous early Miocene Cephalomyidae gen. indet. sp. indet. (Dozo, 1997b) and *Hypsosteiromys* (Dozo et al., 2004) could not be determined because their endocranial volumes are not available. Compared with living caviomorphs (except for *Capromys* Desmarest, 1822), *Prospaniomys* has a lower EQ. However, we need to note that *Hydrochoerus* and *Lagostomus maximus* (Desmarest, 1817) have lower EQs than *Prospaniomys* when values were obtained with Eisenberg's equation. Regarding Paleogene noncaviomorph rodents, *Prospaniomys* has a relatively low EQ compared with the Eocene *Paramys* and *Rapamys*, and the early Oligocene *Ischyromys* and *Cedromus* (Fig. 8; Table 2). However, *Prospaniomys* has similar EQs to the middle Eocene *Pseudotomus* (Fig. 8.1–8.3; Table 2).

In addition to the EQ, the relation between endocranial mass and body mass was explored (Fig. 8.4). *Propaniomys* presents an endocranial mass below the value expected for its body mass but falls within the lower range of the extant caviomorphs (Fig. 8.4). *Hydrochoerus* is the taxon with the highest endocranial mass (but it also has a higher body mass). In comparison with noncaviomorphs, *Prospaniomys* presents a lower endocranial mass in relation to its body mass (Fig. 8.4), which is consistent with that observed in the EQ analyses.

Discussion

This study describes for the first time the cranial endocast of a pan-octodontoid and, at the same time, the oldest encephalon of a caviomorph rodent based on a virtual 3D endocast (Figs. 4, 5, 9). *Prospaniomys* has a cranial endocast with all of its elements (i.e., olfactory bulbs, cerebral hemispheres, and cerebellum) anteroposteriorly aligned and a generalized lissencephalic cerebrum. It also has part of the tectum of the mesencephalon exposed and a well-developed vermis of the cerebellum (Fig. 4), characters considered ancestral for rodents (Dechaseaux, 1958; Jerison, 1973; Pilleri et al., 1984; Dozo, 1997b; Bertrand and Silcox, 2016).

Lissencephalic cerebra are proposed to be present in ancestral mammals but also in small mammals with encephalons < 5 g (Pilleri et al., 1984; Macrini et al., 2007; Bertrand and Silcox, 2016; but see Dechaseaux, 1958). However, caviomorph cerebral patterns are variable and diverse, and not all taxa follow the above-mentioned mammalian rule. There are rodents with lissencephalic, gyrencephalic, and also intermediate patterns (Pilleri et al., 1984; Dozo, 1997a, b; Dozo et al., 2004; Madozzo-Jaén, 2019; Ferreira et al., 2020, 2021). *Prospaniomys* is a small rodent with an encephalic mass estimated at 2.3 g (Table 2) and a lissencephalic cerebrum with a few, very shallow sulci. *Cavia*, *Dolicavia*, and *Prodolichotis* are medium-sized cavioids with clearly gyrencephalic cerebra and encephalic masses close to 5 g, whereas erethizontids are medium-sized to large caviomorphs

https://doi.org/10.1017/jpa.2022.98 Published online by Cambridge University Press

with lissencephalic cerebra (Table 2; see Madozzo-Jaén, 2019, for information about *Prodolichotis*). Thus, it is evident that the neocortical complexity in caviomorphs needs to be further evaluated, and that the lissencephalic pattern of *Prospaniomys* could be related to its ancestrality and/or its small size.

The rhomboidal cerebral morphology of *Prospaniomys*, with the temporal lobes laterally expanded, is similar to the morphology present in the early Miocene Cephalomyidae gen. indet. sp. indet. and in *Chinchilla* (Dozo, 1997b; Ferreira et al., 2020; Fig. 5). Cavioids also have a rhomboidal general morphology, but it is more complex owing to the presence of gyrencephalic cerebra with a more expanded anterior cerebral portion (Pilleri et al., 1984; Dozo, 1997b; Madozzo-Jaén, 2019; Ferreira et al., 2020, 2021; Fig. 5). Dozo (1997b) proposed that morphological similarities between Cephalomyidae gen. indet. sp. indet. and *Chinchilla* could reflect close phylogenetic affinities between Chinchilloidea and Cephalomyidae. Indeed, recent phylogenetic analyses partly support this hypothesis because they indicate that cephalomyids are closely related to both Chinchilloidea and also Cavioidea (Boivin et al., 2019; Busker et al., 2020). Because *Prospaniomys* is not closely related to any of these three caviomorph lineages (Fig. 1), its similarities in encephalic morphology do not express phylogenetic relationships. We favor the idea that lissencephalic and rhomboidal cerebra with more expanded temporal lobes could represent the ancestral condition of at least several caviomorph lineages, which is today retained in some taxa (i.e., *Chinchilla*).

Prospaniomys also has the olfactory bulbs and mesencephalon not dorsally covered by the cerebral hemispheres, characters considered ancestral for rodents (Dechaseaux, 1958; Jerison, 1973; Dozo, 1997b; Bertrand and Silcox, 2016; Bertrand et al., 2019).

The vermis, cerebellar hemispheres, and paraflocculi are conspicuous and well developed within the cerebellum. This portion of the encephalon is a center that integrates most sensory and proprioceptive inputs and motor outputs and therefore coordinates the body by regulating muscle tone and the correct function of the joints (Liem et al., 2001; Evans and de Lahunta, 2013). The vermis is larger than the cerebellar hemispheres, an ancestral character for rodents sensu Deschaseaux (1958) and Dozo (1997b). The cerebellar hemispheres have shallow sulci, which indicates the presence of a slightly complex cerebellar morphology, like in the ancestral squirrel *Cedromus* but unlike that observed in the Paleogene fossils *Paramys* and *Ischyromys*, which have smooth surfaces (Fig. 5). The laterally placed paraflocculi are housed in the subarcuate fossa from the petrosal bone and are related to the semicircular canals of the inner ear, playing a role in head posture and the control of eye movements in mammals (McClure and Daron, 1971; Jeffery and Spoor, 2006). Bertrand et al. (2017, 2019, 2021) related the complex morphology of the cerebellum and the large size of the paraflocculi in the early Oligocene *Cedromus* to improvements in vision and/or balance and limb coordination related to the transition to arboreality in squirrels.

From a paleobiological point of view, the general studies performed here indicate that *Prospaniomys* has relatively small olfactory bulbs, which could be an indication of no olfaction-dependent habits (e.g., arboreal, diurnal, aquatic; Barton et al., 1995; Bertrand et al., 2021). In addition, *Prospaniomys* has relatively low endocranial volume and degree of neocorticalization, which are related to a simpler lifestyle because the neocortex is the main place of sensory integration and high-level processing of different stimuli (Liem et al., 2001; Kardong, 2012). In addition, the relative size of the paraflocculi and the poor posterior extension of the posterior part of the cerebral hemispheres (= visual part; Campos and Welker, 1976; Quiroga, 1988; Krubitzer et al., 2011) led us to discard vision-dependent capacities. Based on Bertrand et al. (2021), the above characters would be more compatible with fossorial and scansorial habits, discarding arboreal and gliding habits. However, *Prospaniomys* has relatively large paraflocculi, which are not expected in fossorial rodents because they have smaller paraflocculi (e.g., *Aplodontia rufa* Rafinesque, 1817; Bertrand et al., 2018, 2021). In addition, *Prospaniomys* has bunolophodont cheek teeth and delicate incisors, characters not present in rodents that burrow, live underground, or are exposed to high dust levels (Agrawal, 1967; Gomes Rodrigues, 2015; Madden, 2015). Thus, the above-mentioned characteristics are in accordance with the generalized terrestrial habits proposed for *Prospaniomys* (Álvarez and Arnal, 2015; Arnaudo et al., 2020).

Based on encephalic size and generalized morphology, and taking into account its phylogenetic position within Pan-Octodontoidea, we infer that the character combination present in *Prospaniomys* could be related to ancestry, at least, for crown pan-octodontoids (Fig. 1). As mentioned above, these characters could be interpreted as ancestral also for other caviomorph lineages (e.g., at least some cephalomyids and chinchilloids). However, it is important to note that by the early Miocene, erethizontids had different and conservative encephalic morphologies (Dozo et al., 2004) and that by the late Miocene, the dinomyid *Neoepiblema* also had derived aspects in the encephalon (Ferreira et al., 2020). Thus, we observed that by the Miocene, caviomorphs presented a wide array of encephalic morphologies, several considered more ancestral and others more derived. This relatively high morphological diversity could be related to the group's high taxonomic and ecological diversity (Vucetich et al., 2015a). In this regard, it would be interesting to study whether this diversity is associated with the main radiation events observed for caviomorphs (e.g., Pérez and Pol, 2012; Verzi et al., 2014; Arnal and Vucetich, 2015; Álvarez et al., 2017; Boivin et al., 2019; Busker et al., 2020; Rasia et al., 2021), or more related to ecological factors, or both. However, the above-mentioned scarce neuroanatomical information available for fossil caviomorphs does not permit us to establish strong evolutionary hypotheses about neuroanatomical aspects. In addition, several works have stated that some ecological aspects, e.g., locomotor behavior, have strongly molded the encephalon in rodents (Bertrand et al., 2021). Thus, more studies of ancient caviomorphs are needed to corroborate these assumptions.

Encephalization quotient.—The EQ has been used as a measure to explore how mammalian encephalic sizes have varied along their evolutionary history (Jerison, 1973; Pilleri et al., 1984; Bertrand et al., 2016b). In this work, we made comparisons between *Prospaniomys* and other Paleogene noncaviomorph rodents and also a few fossils and living caviomorphs, to observe the evolution of the encephalon through time (Fig. 8; Table 2).

https://doi.org/10.1017/jpa.2022.98 Published online by Cambridge University Press

According to Jerison (1973), there is a temporal effect on encephalic size, in which ancestral mammals had small encephalons, and more derived taxa increased their encephalic size through time owing to different ecological pressures. This hypothesis was tested and supported in several mammalian groups (Radinsky, 1976; Silcox et al., 2010; Orliac and Glissen, 2012; Yao et al., 2012). However, Bertrand and Silcox (2016) and Bertrand et al. (2019, and literature cited therein) stated that for rodents, this seems not to be the case. Our observations agree with the latter proposals at least for rodents in general because *Prospaniomys* is considerably younger than the Paleogene noncaviomorph rodents (~10 Ma younger), and has a lower EQ. Nevertheless, *Prospaniomys* belongs to a different rodent lineage (= Ctenohystrica) than the Paleogene noncaviomorph forms (= Ischiromyiformes; Marivaux et al., 2004), and the observed EQ differences could reflect variations in the development in the encephalon that occurred at different ratios between the two groups. However, within fossil caviomorphs, we observed a small reduction in the EQ in two late early and late Miocene taxa (*Neoreomys* and *Neoepiblema*), and then an increase in the late Pliocene (*Dolicavia*) through the Recent (Fig. 8; Table 2). These fossil caviomorphs are in different clades (i.e., Pan-Octodontoidea, Cavioidea, and Chinchilloidea) and perhaps the observed EQ distributions reflect the isolated evolution of these caviomorph lineages. Within Pan-Octodontoidea, *Prospaniomys* has an expected lower EQ than the living taxa (with the exception of *Capromys*), which could be reasonably inferred by its antiquity.

Pilleri et al. (1984) postulated that the EQ is related to ecological, behavioral, and/or physiological factors. These authors concluded that lower EQs are consistent with terrestrial habits of animals that lived in large communities in open, unprotected environments. Many of these factors cannot be inferred precisely for fossil species, but the low EQ of *Prospaniomys* is consistent with the terrestrial habits inferred by its encephalic morphology (see discussion above) and by Álvarez and Arnal (2015).

Conclusions

The virtual 3D endocast of the early Miocene *Prospaniomys priscus* from Argentinean Patagonia sheds light on the neuroanatomy of pan-octodontoids, and leads to comparisons with other South American Hystricognathi and several Paleogene noncaviomorph rodents. *Prospaniomys* has an encephalic morphology that we consider ancestral for Pan-Octodontoidea and other caviomorph lineages (e.g., several cephalomyids, chinchillids) characterized by: (1) aligned anteroposterior elements, (2) the rhombic cerebral hemispheres with well-developed and laterally expanded temporal lobes, (3) part of the tectum of the mesencephalon exposed, and (4) the well-developed vermis of the cerebellum. In addition, *Prospaniomys* has relatively small olfactory bulbs, relative large paraflocculi of the cerebellum, and low endocranial volume and degree of neocorticalization. The EQ of *Prospaniomys* is lower compared to several Paleogene noncaviomorph rodents (i.e., *Paramys*, *Rapamys*, and *Cedromus*), but is slightly higher than in other late early and late Miocene caviomorphs (i.e., *Neoreomys* and *Neoepiblema*), a striking feature that needs to be further studied. The neuroanatomical information supports the hypothesis that *Prospaniomys* was a terrestrial, generalist caviomorph rodent, with no complex or vision-dependent habits.

Besides the scarce caviomorph endocranial information, by the Miocene, we observed high diversity of encephalic morphologies (each fossil taxon with a different encephalic bauplan). This could be related to the main radiation events observed for caviomorphs and could indicate that most encephalic characters change following different ecological pressures in each caviomorph lineage, agreeing with the proposal of Bertrand et al. (2021).

The limited endocranial fossil caviomorph samples are a problem to providing conclusive observations on most aspects. The present work and previous contribution (Arnaudo et al., 2020) are far from providing quantitative comparisons within and between taxa. However, these advances provide an enormous amount of information and, for the first time, shed light on the anatomy and evolution of several paleoneurological aspects for this particular group of South American rodents. This new endocast information increases the database knowledge that can be used in phylogenetic analyses.

Acknowledgments

To L. Chornogubsky and M. Ezcurra (MACN) for allowing study of the fossil specimen under their care. To the Y-TEC and B. Epele (Y-TEC) for the good predisposition in allowing us to scan the fossil specimen. To P. Bona (Museo de La Plata) for discussion on anatomical concepts. To J. Taborda and J. Tavella for advice on methodological aspects. To the reviewers (O. Bertrand and M. Boivin) and to the editors of the Journal of Paleontology (J. Calede and H.-D. Sues) for their revisions and suggestions that substantially improved the manuscript. Thanks to the financial support of the Bunge & Born Foundation to the corresponding author.

Declaration of competing interests

The authors declare none.

Data availability statement

Supplementary data for this study are available in the Dryad Digital Repository: https://doi.org/10.5061/dryad.70rxwdc27.

References

Agrawal, V.C., 1967, Skull adaptations in fossorial rodents. Mammalia: v. 31, p. 300–312.

Álvarez, A., and Arnal, M., 2015, First approach to the paleobiology of the extinct *Prospaniomys* (Rodentia, Hystricognathi, Octodontoidea) through head muscle reconstruction and the study of craniomandibular shape variation: Journal of Mammalian Evolution, v. 22, p. 519–533, https://doi.org/10.1007/s10914-015-9291-z.

Álvarez, A., and Ercoli, M.D., 2017, Why pacaranas never say no: Analysis of the unique occipitocervical configuration of *Tetrastylus intermedius* Roverето, 1914, and other dinomyids (Caviomorpha, Dinomyidae): Journal of Vertebrate Paleontology, v. 37, no. 6, https://doi.org/10.1080/02724634.2017.1385476.

Álvarez, A., Moyers Arévalo, R.L., and Verzi, D.H., 2017, Diversification patterns and size evolution in caviomorph rodents: Biological Journal of the

Linnean Society, v. 121, p. 907–922, http://doi.org/10.1093/biolinnean/blx026.
Ameghino, F., 1887, Enumeración sistemática de las especies de mamíferos fósiles coleccionadas por Carlos Ameghino en los terrenos eocenos de la Patagonia austral: Boletín del Museo de La Plata, v. 1, p. 1–26.
Ameghino, F., 1888, Lista de especies de mamíferos fósiles del Mioceno Superior de Monte Hermoso, hasta ahora conocidas: Buenos Aires, Coni, P.E. e Hijos, 21 p.
Ameghino, F., 1889, Contribución al conocimiento de los mamíferos fósiles de la República Argentina: Actas de la Academia Nacional de Ciencias en Córdoba, v. 6, p. 1–1027.
Ameghino, F., 1897, Mammifères Crétacés de l'Argentine: Deuxième contribution à la connaissance de la faune mammalogique dês couches à Pyrotherium: Boletín del Instituto Geográfico Argentino, v. 18, p. 406–429, 431–521.
Ameghino, F., 1902, Première contribution à la connaissance de la faune mammalogique des couches à *Colpodon*: Boletín de la Academia Nacional de Ciencias de Córdoba, v. 17, p. 71–138.
Ameghino, F., 1908, Las formaciones sedimentarias de la región litoral de Mar del Plata y Chapadmalal: Anales del Museo Nacional de Buenos Aires, v. 10, p. 343–423.
Ameghino, C., 1916, *Dolicavia* nov. gen. de Caviidae (Roedores) del Chapalmalense de Miramar (Provincia de Buenos Aires): Physis, v. 2, p. 283–284.
Antoine, P.-O., Marivaux, L., Croft, D.A., Billet, G., Ganerod, M., Grégory Fanjat, C., Rousse, S., and Salas-Gismondi, S., 2012, Middle Eocene rodents from Peruvian Amazonia reveal the pattern and timing of caviomorph origins and biogeography: Proceedings of the Royal Society, B, Biological Sciences, v. 279, p. 1319–1326, https://doi.org/10.1098/rspb.2011.1732.
Argyle, E.C., and Mason, M.J., 2008, Middle ear structures of *Octodon degus* (Rodentia, Octodontidae), in comparison with those of subterranean caviomorphs: Journal of Mammalogy, v. 89, p. 1447–1455, https://doi.org/10.1644/07-MAMM-A-401.1.
Arnal, M., 2012, Sistemática, filogenia e historia evolutiva de roedores Octodontoidea (Caviomorpha, Hystricognathi) del Oligoceno tardío-Mioceno medio vinculados al origen de la familia Octodontidae [Ph.D. dissertation]: La Plata, Argentina, Universidad Nacional de La Plata, http://naturalis.fcnym.unlp.edu.ar/id/20120426001230 (accessed August 2022).
Arnal, M., and Kramarz, A.G., 2011, First complete skull of an octodontoid (Rodentia, Caviomorpha) from the early Miocene of South America and its bearing in the early evolution of Octodontoidea: Geobios, v. 44, p. 435–444, https://doi.org/10.1016/j.geobios.2010.12.003.
Arnal, M., and Vucetich, M.G., 2015, Main radiation events in Pan-Octodontoidea (Rodentia, Caviomorpha): Zoological Journal of the Linnean Society, v. 175, p. 587–606, https://doi.org/10.1111/zoj.12288.
Arnal, M., Kramarz, A.G., Vucetich, M.G., and Vieytes, C.E., 2014, A new early Miocene octodontoid rodent (Hystricognathi, Caviomorpha) from Patagonia (Argentina) and a reassessment of the early evolution of Octodontoidea: Journal of Vertebrate Paleontology, v. 34, no. 2, p. 397–406, https://doi.org/10.1080/02724634.2013.808203.
Arnal, M., Kramarz, A.G., Vucetich, M.G., Frailey, C.D., and Campbell, K.E. Jr., 2020, New Paleogene caviomorphs (Rodentia, Hystricognathi) from Santa Rosa, Peru: Systematics, biochronology, biogeography and early evolutionary trends: Papers in Palaeontology, v. 6, p. 193–216, https://doi.org/10.1002/spp2.1264.
Arnal, M., Pérez, M.E., Tejada Medina, L.M., and Campbell, K.E. Jr., 2022, The high taxonomic diversity of the Paleogene hystricognath rodents (Caviomorpha) from Santa Rosa (Peru, South America) framed within a new geochronological context: Historical Biology, v. 2022, p. 1–24, https://doi.org/10.1080/08912963.2021.2017916.
Arnaudo, M.E., Arnal, M., and Ekdale, E.G., 2020, The auditory region of a caviomorph rodent (Hystricognathi) from the early Miocene of Patagonia (South America) and evolutionary considerations: Journal of Vertebrate Paleontology, v. 40, no. 2, https://doi.org/10.1080/02724634.2020.1777557.
Barton, R.A., Purvis, A., and Harvey, P.H., 1995, Evolutionary radiation of visual and olfactory brain systems in primates, bats and insectivores: Philosophical Transactions of The Royal Society, B, Biological Sciences, v. 348, p. 381–392.
Bennet, E.T., 1829, The chinchilla, *in* Bennett, E.T., ed., Gardens and Menagerie of the Zoological Society Delineated, Quadrupeds, Volume 1: London: Charles Tilt, p. 1–12.
Bertrand, O.C., and Silcox, M.T., 2016, First virtual endocast of a fossil rodent: *Ischyromys typus* (Ischiromyidae, Oligocene) and brain evolution in rodents: Journal of Vertebrate Paleontology, v. 36, no. 3, https://doi.org/10.1080/02724634.2016.1096275.
Bertrand, O.C., Flynn, J.J., Croft, D.A., and Wyss, A.R., 2012, Two new taxa (Caviomorpha, Rodentia) from the early Oligocene Tinguiririca fauna (Chile): American Museum Novitates, v. 3750, p. 1–36, https://doi.org/10.1206/3750.2.
Bertrand, O.C., Schillaci, M.A., and Silcox, M.T., 2016a, Cranial dimensions as estimators of body mass and locomotor habits in extant and fossil rodents: Journal of Vertebrate Paleontology, v. 36, no. 1, p. 1–10, https://doi.org/10.1080/02724634.2015.1014905.
Bertrand, O.C., Amador-Mughal, F., and Silcox, M.T., 2016b, Virtual endocast of eocene *Paramys* (Paramyidae): Oldest endocranial record for Rodentia and early brain evolution in Euarchontoglires: Proceedings of the Royal Society, B, v. 283, no. 1823, p. 1–8, https://doi.org/10.1098/rspb.2015.2316.
Bertrand, O.C., Amador-Mughal, F., and Silcox, M.T., 2017, Virtual endocast of the early Oligocene *Cedromus wilsoni* (Cedromurinae) and brain evolution in squirrels: Journal of Anatomy, v. 230, p. 128–151, https://doi.org/10.1111/joa.12537.
Bertrand, O.C., Amador-Mughal, F., Lang, M.M., and Silcox, M.T., 2018, Virtual endocast of fossil Sciuroidea: Brain size reduction in the evolution of fossoriality: Palaeontology, v. 61, no. 6, p. 919–948, https://doi.org/10.1111/pala.12378.
Bertrand, O.C., Amador-Mughal, F., Lang, M.M., and Silcox, M.T., 2019, New virtual endocasts of Eocene Ischyromyidae and their relevance in evaluating neurological changes occurring through time in Rodentia: Journal of Mammalian Evolution, v. 26, p. 345–371, https://doi.org/10.1007/s10914-017-9425-6.
Bertrand, O.C., Püschel, H.P., Schwab, J.A., Silcox, M.T., and Brusatte, S.L., 2021, The impact of locomotion on the brain evolution of squirrels and close relatives. Communications Biology, 4, no. 1, p. 1–15, https://doi.org/10.1038/s42003-021-01887-8.
Bocquentin, J., Filho, J.P.S., and Negri, F.R., 1990, *Neoepiblema acreensis*, sp. n. (Mammalia, Rodentia) do Neogeno do Acre, Brasil: Boletim do Museu Paraense Emilio Goeldi, Serie Ciencias da Terra, v. 2, p. 65–72.
Boivin, M., Ginot, S., Marivaux, L., Altamirano-Sierra, A.J., Pujos, F., Salas-Gismondi, R., Tejada-Lara, J.V., and Antoine, P.-O., 2018, Tarsal morphology and locomotor adaptation of some late middle Eocene caviomorph rodents from Peruvian Amazonia reveal early ecological diversity: Journal of Vertebrate Paleontology, v. 38, no. 6, https://doi.org/10.1080/02724634.2018.1555164.
Boivin, M., Marivaux, L., and Antoine, P.-O., 2019, L'apport du registre paléogène d'Amazonie sur la diversification initiale des Caviomorpha (Hystricognathi, Rodentia): Implications phylogénétiques, macroévolutives et paléobiogéographiques: Geodiversitas, v. 41, p. 143–245, https://doi.org/10.5252/geodiversitas2019v41a4.
Brisson, M.J., 1762, Regnum Animale in Classes 9, Lugduni Batavorum: Leiden, Theordorum Haak, 294 p.
Brookes, J., 1829, On a new genus of the order Rodentia: Transactions of the Linnean Society, v. 16, no. 1, p. 95–104.
Bugge, J. 1985, Systematic value of the carotid arterial pattern in rodents, *in* Luckett, W.P., and Hartenberger, J.-J., eds., Evolutionary Relationships Among Rodents: A Multidisciplinary Analysis (NATO ASI Series): New York, Plenum Press, p. 355–379.
Busker, F., Dozo, M.T., and Soto, I.M., 2020, New remains of *Cephalomys arcidens* (Rodentia, Caviomorpha) and a redefinition of the enigmatic Cephalomyidae: Journal of Systematic Palaeontology, v. 18, no. 19, p. 1589–1629, https://doi.org/10.1080/14772019.2020.1796833.
Campos, G.B., and Welker, W.I., 1976, Comparisons between brains of a large and a small hystricomorph rodent: Capybara, *Hydrochaeris* and guinea pig, *Cavia*: Neocortical projection regions and measurements of brain subdivisions: Brain, Behavior and Evolution, v. 13, no. 4, p. 243–266.
Candela, A.M., Rasia, L.L., and Pérez, M.E., 2012, Paleobiology of Santacrucian caviomorph rodents: A morphofunctional approach, *in* Vizcaíno, S.F., Kay, R.F., and Bargo, M.S., eds., Early Miocene Paleobiology in Patagonia: High-Latitude Paleocommunities of the Santa Cruz Formation: Cambridge, UK, Cambridge University Press, p. 287–305.
Cope, E.D., 1872, Second account of new Vertebrata from the Bridger Eocene: American Philosophical Society, v. 12, p. 466–468.
Croft, D.A., 2000, Archaeohyracidae (Mammalia, Notoungulata) from the Tinguiririca Fauna, central Chile, and the evolution and paleoecology of South American mammalian herbivores [Ph.D. dissertation]: Chicago, University of Chicago, 327 p.
Cuvier, F., 1823a, Examen des espèces du genre porc-épic, et formation des genres ou sous- genres *Acanthion*, *Eréthizon*, Sinéthère et Sphiggure: Mémoires du Muséum National d'Histoire Naturelle, v. 9, p. 413–437.
Cuvier, F., 1823b, Sur les rapports qui existent entre les animaux de la famille des Écureuils; c'est-à-dire, les Tamias, les Macroxus, les Ecureuils, les Sciuroptères et les Ptéromys: Mémoires du Museum National d'Histoire Naturelle de Paris, v. 10, p. 116–128.
Dechaseaux, C., 1958, Encéphales des Simplicidentés fossiles, *in* Piveteau, J., ed., Traité de Paléontologie: Paris, Masson et Cie, p. 819–821.
Desmarest, A.G., 1817, Le grande gerboise, *Dipus maximus*, Blainv.: Nouveau Dictionnaire d'Histoire Naturelle, v.13, p. 117–119.
Desmarest, A.G., 1819, Note sur un mammifère de l'ordre Rongeurs, mentionné par quelques auteurs, mais dont l'existence n'est pas encore généralment

https://doi.org/10.1017/jpa.2022.98 Published online by Cambridge University Press

admise par les Signaturalistes nomenclateurs: Journal de Physique, de Chimie, d'Histoire Naturelle et des Arts, v. 88, p. 205–211.
Desmarest A.G., 1822, Mammalogie ou description des espèces de mammifères, seconde partie, contenant les orders de Rongeurs, des Édentés, des Pachydermes, des Ruminans et des Cetacés, Part 2: Paris, Veuve Agasse, Encyclopédie Méthodique, p. 277–555.
Dozo, M.T., 1997a, Paleoneurología de *Dolicavia minuscula* (Rodentia, Caviidae) y *Paedotherium insigne* (Notoungulata, Hegetotheriidae) del Plioceno de Buenos Aires, Argentina: Ameghiniana, v. 34, p. 427–435.
Dozo, M.T., 1997b, Primer estudio paleoneurológico de un roedor caviomorfo (Cephalomyidae) y sus posibles implicancias filogenéticas: Mastozoología Neotropical, v. 4, p. 89–96.
Dozo, M.T., and Martínez, G., 2016, First digital cranial endocast of late Oligocene Notohippidae (Notoungulata): Implications for endemic South American ungulates brain evolution: Journal of Mammalian Evolution, v. 23, p. 1–16, https://doi.org/10.1007/s10914-015-9298-5.
Dozo, M.T., Vucetich, M.G., and Candela, A.M., 2004, Skull anatomy and neuromorphology of *Hypsosteiromys*, a colhuehuapian erethizontid rodent from Argentina: Journal of Vertebrate Paleontology, v. 24, p. 228–234, https://doi.org/10.1671/18.1.
Eisenberg, J.F., 1981, The Mammalian Radiations: An Analysis of Trends in Evolution, Adaptation, and Behavior: Chicago, University of Chicago Press, 610 p.
Erxleben, J.C.P., 1777, Systema Regni Animalis per Classes, Ordines, Genera, Species, Varietates cum Synonymia et Historia Animalium, Classis 1, Mammalia: Lipsiae, Impensis Weygandianis, 636 p.
Evans, H.E., and de Lahunta, A., 2013, Miller's Anatomy of the Dog (fourth edition): St. Louis, Missouri, Elsevier Health Sciences, 872 p.
Fedorov, A., Beichel, R., Kalpathy-Cramer, J., Finet, J., Fillion-Robin, J.-C., Pujol, S., Bauer, C., Jennings, D., Fennessy, F.M., Sonka, M., Buatti, J., Aylward, S.R., Miller, J.V., Pieper, S., and Kikinis, R., 2012, 3D Slicer as an image computing Platform for the 60 Quantitative Imaging Network: Magnetic Resonance Imaging, v. 30, p. 1323–1341, https://doi.org/10.1016/j.mri.2012.05.001.
Fernández-Monescillo, M., Antoine, P.-O., Pujos, F., Gomes Rodrigues, H., Mamani Quispe, B., and Orliac, M., 2019, Virtual endocast morphology of Mesotheriidae (Mammalia, Notoungulata, Typotheria): New insights and implications on notoungulate encephalization and brain evolution: Journal of Mammalian Evolution, v. 26, p. 85–100, https://doi.org/10.1007/s10914-017-9416-7.
Ferreira, J.D., Negri, F.R., Sánchez-Villagra, M.R., and Kerber, L., 2020, Small within the largest: Brain size and anatomy of the extinct *Neoepiblema acreensis*, a giant rodent from the Neotropics: Biological Letters, v. 16, no. 20190914, https://doi.org/10.1098/rsbl.2019.0914.
Ferreira, J.D., Dozo, M.T., De Moura Bubadué, J., and Kerber, L., 2021, Morphology and postnatal ontogeny of the cranial endocast and paranasal sinuses of capybara (*Hydrochoerus hydrochaeris*), the largest living rodent: Journal of Morphology, v. 283, p. 1–25, https://doi.org/10.1002/jmor.21428.
Fleagle, J.G., and Bown, T.M., 1983, New primate fossil from the late Oligocene (Colhuehuapian) localities of Chubut Province, Argentina: Folia Primatologica, v. 41, p. 240–266.
Frailey, C.D., and Campbell, K.E., 2004, Paleogene rodents from Amazonian Peru: The Santa Rosa local fauna, *in* Campbell, K.E., ed., The Paleogene Mammalian Fauna of Santa Rosa, Amazonian Peru: Natural History Museum of Los Angeles County, Science Series, v. 40, p. 71–130.
Freudenthal, M., and Martín-Suárez, E., 2013, Estimating body mass of fossil rodents: Scripta Geologica, v. 145, p. 1–513.
Gingerich, P.D., and Gunnel, G.F., 2005, *Brain of* Plesiadapis cookie *(Mammalia, Proprimates): Surface morphology and encephalization compared to those of primates and Dermoptera*: Contributions from the Museum of Paleontology of the University of Michigan, v. 31, no. 8, p. 185–195.
Gomes Rodrígues, H., 2015, The great variety of dental structures and dynamics in rodents: New insights into their ecological diversity, *in* Cox, P.G., and Hautier, L., eds., Evolution of the Rodents: Advances in Phylogeny, Functional Morphology and Development: Cambridge, UK, Cambridge University Press, p. 424–447.\
Gray, J.E., 1842, Descriptions of some new genera and fifty unrecorded species of Mammalia: Annals and Magazine of Natural History, ser. 1, v. 10, p. 255–267.
Hammer, Ø., Harper, D.A.T., and Ryan, P.D., 2001, PAST: Paleontological statistics software package for education and data analysis: Palaeontologia Electronica, v. 4, no. 1, p. 1–9, http://palaeo-electronica.org/2001_1/past/issue1_01.htm (accessed April 2022).
Hensel, R., 1872, Beiträge zur Kentniss der Säugethiere Süd- Brasiliens: Abhandlungen der Königlichen Akademie der Wissenschaftenzu Berlin, v. 1872, p. 1–130.
Hill, J.E., 1935, The cranial foramina in rodents: Journal of Mammalogy, v. 16, no. 2, p. 121–129.
Hoffstetter, R., and Lavocat, R., 1970, Découverte dans le Déséadien de Bolivia de genres pentalophodontes appuyant les affinités africaines des Rongeurs Caviomorphes: Comptes Rendus de l'Académie des Sciences de Paris, v. 271, p. 172–175.
Illiger, J.K.W., 1811, Prodromus Systematis Mammalium et Avium Additis Terminis Zoographicis Utriusque Classis, Eorumque Versione Germanica: Berlin, Berolini, C. Salfield, 302 p.
International Committee on Veterinary Gross Anatomical Nomenclature, 2017, Nomina Anatomica Veterinaria (NAV) (sixth edition): Hanover, Germany, Editorial Committee, 160 p.
Jeffery, N., and Spoor, F., 2006, The primate subarcuate fossa and its relationship to the semicircular canals, Part I: Prenatal growth: Journal of Human Evolution, v. 51, p. 537–549, https://doi.org/10.1016/j.jhevol.2006.07.003.
Jerison, H.J., 1973, Evolution of the Brain and Intelligence: New York, Academic Press, 482 p.
Jerison, H.J., 2012, Digitized fossil brains: neocorticalization: Biolinguistics, v. 6, p. 383–392, https://doi.org/10.5964/bioling.8929.
Kardong, K.V., 2012, Vertebrates: Comparative Anatomy, Function, Evolution (sixth edition); New York, McGraw-Hill, 794 p.
Kerber, L., Candela, A.M., Ferreira, J.D., Pretto, F.A., Bubadué, J., and Negri, F.R., 2022, Postcranial morphology of the extinct rodent *Neopiblema* (Rodentia, Chinchilloidea): Insights into the paleobiology of neopiblemids: Journal of Mammalian Evolution, v. 29, p. 207–235, https://doi.org/10.1007/s10914-021-09567-4.
Kerr, R., 1792, The Animal Kingdom or Zoological System, of the Celebrated Sr. Charles Linnaeus, Class I, Mammalia: Containing a Complete Systematic Description, Arrangement, and Nomenclature, of All Known Species and Varieties of the Mammalia, or Animals which give Suck to their Young; being a Translation of that part of the Systema Naturae, as lately Published, with Great Improvements, by Professor Gmelin of Goettingen: Together with Numerous Additions from More Recent Zoological Writers, and Illustrated with Copperplates: Edinburgh, A. Strahan, T. Cadell, and W. Creech, 400 p.
Köhler, M., and Moyà-Solà, S., 2004, Reduction of brain and sense organs in the fossil insular bovid *Myotragus*: Brain, Behavior and Evolution, v. 63, p. 125–140, https://doi.org/10.1159/000076239.
Korth, W.W., 1984, Earliest Tertiary evolution and radiation of rodents in North America: Bulletin of Carnegie Museum of Natural History, v. 24, p. 1–71.
Korth, W.W., 1994, The Tertiary Record of Rodents in North America (Topics in Geobiology, v. 12): New York, Plenum Press, 339 p.
Korth, W.W., and Emry, R.J., 1991, The skull of *Cedromus* and a review of the Cedromurinae (Rodentia, Sciuridae): Journal of Paleontology, v. 65, p. 984–994.
Kraglievich, L., 1932, Diagnosis de nuevos géneros y especies de roedores cávidos y eumegámidos fósiles de la Argentina: Rectificación genérica de algunas especies conocidas y adiciones al conocimiento de otras: Anales de la Sociedad Científica Argentina, v. 114, p. 155–181, 211–237.
Kramarz, G.A., Vucetich, M.G., and Arnal, M., 2013, A new early Miocene chinchilloid hystricognath rodent: An approach to the understanding of the early chinchillid dental evolution: Journal of Mammalian Evolution, v. 20, no. 3, p. 249–261, https://doi.org/10.1007/s10914-012-9215-0.
Krubitzer, L., Campi, K. L., and Cooke, D.F., 2011, All rodents are not the same: A modern synthesis of cortical organization: Brain, Behavior and Evolution, v. 78, p. 51–93, https://doi.org/10.1159/000327320.
Lacépède, B.G.E. de la V., 1799, Tableau des Divisions, Sous-divisions, Orders et Genres des Mammifères, Supplement to Discours d'Ouverture et de Clôture du Cours d'Histoire Naturelle Donné Dans le Muséum National d'Histoire Naturelle, l'An VII de la République, et Tableau Méthodiques des Mammifères et de Oiseaux: Paris, Plassan, 18 p.
Lavocat, R., and Parent, J.-P., 1985, Phylogenetic analysis of middle ear features in fossil and living rodents, *in* Luckett, W.P., and Hartenberger, J.-J., eds., Evolutionary Relationships Among Rodents: A Multidisciplinary Analysis (NATO ASI Series): New York and London, Plenum Press, p. 333–354.
Legendre, S., 1986, Analysis of mammalian communities from the late Eocene and Oligocene of southern France: Palaeovertebrata, v. 16, no. 4, p. 191–212.
Leidy, J., 1856, Notices of remains of extinct Mammalia discovered by Dr. F. V. Hayden in Nebraska Territory: Proceedings of the Academy of Natural Sciences of Philadelphia, v. 8, p. 88–90.
Leidy, J., 1871, Notice of some extinct rodents: Proceedings of the Academy of Natural Sciences of Philadelphia, v. 22, p. 230–232.
Lichtenstein, H., 1823, Verzeichniss der Doubletten des Zoologischen Museums der Königl. Universität zu Berlin nebst Beschreibung vieler bisher unbekannter Arten von Säugethieren, Vögeln, Amhibien und Fischen: Berlin, Doubletten Zoologischen Museums, 118 p.
Liem, K., Bernis, W., Walker, W.F., and Grande, L., 2001, Functional Anatomy of the Vertebrates: An Evolutionary Perspective (third edition): Belmont, California, Brooks/Cole, Thompson Learning, 759 p.

Linnaeus, C., 1758, Systema Naturae per Regna Tria Naturae (tenth edition), Volume 1, Regnum Animale: Stockholm, Laurentii Salvii, 824 p
Linnaeus, C., 1766, Systema Naturae per Regna Tria Naturae, Secundum Classes, Ordines, Genera, Species, cum Characteribus, Differentiis, Synonymis, Locis (editio duodecima, reformata): Vienna, Typis Ioannis Thomae, 532 p.
Loomis, F.B., 1907, Wasatch and Wind River rodents: American Journal of Science, ser. 4, v. 23, p. 123–130.
Lund, P.W., 1839, Coup-d'oeil sur le espèces éteintes de mammifères du Brésil: Extrait de quelques mémoires présentés à l'Academie royale des Sciences de Copenhague: Annales des Sciences Naturelles (Paris), ser. 2, v. 11, p. 214–234.
Macrini, T.E., Rowe, T., and Archer, M., 2006, Description of a cranial endocast from a fossil platypus, *Obdurodon dicksoni* (Monotremata, Ornithorhynchidae), and the relevance of endocranial characters to monotreme monophyly: Journal of Morphology, v. 267, p. 1000–1015, https://doi.org/10.1002/jmor.10452.
Macrini, T.E., Rougier, G.W., and Rowe, T., 2007, Description of a cranial endocast from the fossil mammal *Vincelestes neuquenianus* (Theriiformes) and its relevance to the evolution of endocranial characters in therians: The Anatomical Record, v. 290, p. 875–892, https://doi.org/10.1002/ar.20551.
Madden, R.H., 2015, Hypsodonty in Mammals: Evolution, Geomorphology, and the Role of Earth Surface Processes: Cambridge, UK, Cambridge University Press, 423 p.
Madozzo-Jaén, M.C., 2019, Systematic and phylogeny of *Prodolichotis prisca* (Caviidae, Dolichotinae) from the northwest of Argentina (late Miocene–early Pliocene): Advances in the knowledge of the evolutionary history of maras: Comptes Rendus Palevol, v. 18, no. 1, p. 33–50, https://doi.org/10.1016/j.crpv.2018.07.003.
Marivaux, L., Vianey-Liaud, M., and Jaeger, J.-J., 2004, High-level phylogeny of early Tertiary rodents: Dental evidence: Zoological Journal of the Linnean Society, v. 142, p. 105–134, https://doi.org/10.1111/j.1096-3642.2004.00131.x.
Marsh, O.C., 1872, Preliminary description of new Tertiary mammals: American Journal of Science, v. 4, p. 202–224.
Mason, M.J., 2015, Functional morphology of rodent middle ears, *in* Cox, P.G., and Hautier, L., eds., Evolution of the Rodents: Advances in Phylogeny, Functional Morphology and Development: Cambridge, UK, Cambridge University Press, p. 373–404.
Matthew, W.D., 1910, On the osteology and relationships of *Paramys* and the affinities of the Ischyromyidae: Bulletin of the American Museum of Natural History, v. 28, p. 43–71.
Matthew, W.D., 1920, A new genus of rodents from the middle Eocene: Journal of Mammalogy, vol. 1, no. 4, p. 168, 169.
McClure, D.T., and Daron, G.H., 1971, The relationship of the developing inner ear, subarcuate fossa and paraflocculus in the rat: American Journal of Anatomy, v. 130, p. 235–250.
Meyen, F.J.F., 1833, Beiträge zur Zoologie, gesammelt auf einer Reise um die Erde, Zweite Abhandlung, Säugethiere: Nova Acta Physico Medica Academiea Caesareae Leopoldino- Carolinae Naturae Curiosorum, v. 16, p. 549–610.
Molina, G.I., 1782, Saggio Sulla Storia Naturale del Chili (first edition): Bologna, Stamperia di San Tomnaso d'Aquino, 368 pp.
Novacek, M.J., 1986, The skull of *Lepticif insectivorans* and the higher-level classification of eutherian mammals: Bulletin of the American Museum of Natural History, v. 183, p. 1–112.
Orliac, M.J, and Gilissen, E., 2012, Virtual endocranial cast of earliest Eocene *Diacodexis* (Artiodactyla, Mammalia) and morphological diversity of early artiodactyl brains: Proceedings of the Royal Society, B, Biological Sciences, v. 279, p. 3670–3677, https://doi.org/10.1098/rspb.2012.1156.
Osborn, H.F., 1908, New fossil mammals from the Fayûm Oligocene, Egypt: Bulletin of the American Museum of Natural History, v. 24, no. 16, p. 265–272.
Osgood, W.H., 1914, Four new mammals from Venezuela: Field Museum of Natural History Zoological Series, v. 10, p. 135–141.
Pallas, P.S., 1766, Miscellanea Zoologica Quibus Novae Imprimis Atque Obscurae Animalium Species Descriuntur et Observationibus Iconibusque Illustrantur: The Hague, P. van Cleef, 224 p.
Pascual, R., 1967, Los roedores Octodontoidea (Caviomorpha) de la Formación Arroyo Chasicó (Plioceno inferior) de la Provincia de Buenos Aires: Revista del Museo de La Plata, Seccion Paleontología, v. 5, p. 259–282.
Patterson, B., 1958, A new genus of erethizontid rodents from the Colhuehuapian of Patagonia: Breviora, v. 92, p. 1–4.
Patterson, B., and Pascual, R., 1968, New echimyids rodents from the Oligocene of Patagonia and a synopsis of the family: Breviora, v. 301, p. 1–14.
Patterson, B., and Wood, A.E., 1982, Rodents from the Deseadan Oligocene of Bolivia and the relationships of the Caviomorpha: Bulletin of the Museum of Comparative Zoology, v. 149, p. 371–543.
Patton, J.L., Pardiñas, U.F., and D'Elía, G., 2015, Mammals of South America, Volume 2, Rodents: Chicago, University of Chicago Press, 1384 p.
Pérez, M.E., and Pol, D., 2012, Major radiations in the evolution of caviid rodents: Reconciling fossils, ghost lineages, and relaxed molecular clocks: PLoS ONE, v. 7, no. 10, e48380, https://doi.org/10.1371/journal.pone.0048380.
Peters, W., 1873, Über *Dinomys* eine merkwürdige neue Gattung der tachelschweinartigen Nagethiere aus den Hochgebirgen von Peru: Monatsberichte der Königlichen Preussischen Akademie der Wissenschaften zu Berlin, v. 1873, p. 551, 552.
Pilleri, G., Gihr, M., and Kraus, C., 1984, Cephalization in rodents with particular reference to the Canadian beaver (*Castor canadensis*), *in* Pilleri, G., ed., Investigations on Beavers: Berne, Switzerland, Brain Anatomy Institute, p. 11–102.
Poux, C., Chevret, P., Huchon, D., de Jong, D.D., and Douzery, E.J.P., 2006, Arrival and diversification of caviomorph rodents and platyrrhine primates in South America: Systematic Biology, v. 55, p. 228–244, https://doi.org/10.1080/10635150500481390.
Quiroga, J.C., 1988, Cuantificación de la corteza cerebral en moldes endocraneanos de mamíferos girencéfalos: Procedimiento y aplicación en tres mamíferos extinguidos: Ameghiniana, v. 25, no. 1, p. 67–84.
Radinsky, L.B., 1968, A new approach to mammalian cranial analysis, illustrated by examples of prosimian primates: Journal of Morphology, v. 124, no. 2, p. 167–179, https://doi.org/10.1002/jmor.1051240204.
Radinsky, L.B., 1976, Early primate brains: Facts and fiction: Journal of Human Evolution, v. 6, p. 79–86.
Rafinesque, C.S., 1817, Descriptions of seven new genera of North American quadrupeds in Museum of Natural Sciences: American Monthly Magazine, v. 2, p. 44–46.
Rasia, L.L., Candela, A.M., and Cañon, C., 2021, Comprehensive total evidence phylogeny of chinchillids (Rodentia, Caviomorpha): Cheek teeth anatomy and evolution: Journal of Anatomy, v. 239, p. 405–423, https://doi.org/10.1111/joa.13430.
Rinderknecht, A., and Blanco, R.E., 2008, The largest fossil rodent: Proceedings of the Royal Society of London, B, Biological Sciences, v. 275, p. 923–928, https://doi.org/10.1098/rspb.2007.1645.
Rovereto, C., 1914, Los estratos araucanos y sus fósiles: Anales del Museo Nacional de Buenos Aires, v. 25, p. 1–247.
Rusconi, C., 1934, Una nueva subespecie de tucu tuco viviente: Revista Chilena de Historia Natural, v. 38, p. 108–110.
Saussure, M.H. de., 1860, Note sur quelques mammifères de Mexique: Revue et Magasin de Zoologie Pure et Appliquée Paris, sèr. 2, no. 12, p. 97–110.
Say, T., 1822,. On the quadruped belonging to the order Rodentia: Proceedings of the Academy of Natural Sciences of Philadelphia, v. 2, p. 333–343.
Silcox, M.T., Benham, A.E., and Bloch, J.I., 2010, Endocasts of *Microsyops* (Microsyopidae, Primates) and the evolution of the brain in primitive primates: Journal of Human Evolution, v. 58, p. 505–521, https://doi.org/10.1016/j.jhevol.2010.03.008.
Trouessart, E.-L., 1897, Catalogus Mammalium tam Viventium Quam Fossilium, Fasciculus 3, Rodentia 2 (Myomorpha, Histricomorpha, Lagomorpha): Berlin, R. Friedländer & Sohn, 664 p.
Tschudi, J.V., 1845, Untersuchungen über die Fauna Peruana, Parts 3–5: St. Gallen, Switzerland, Scheitlin und Zollikofer, p. 77–244.
Upham, N.S., and Patterson, B., 2015, Evolution of caviomorph rodents: A complete phylogeny and timetree for living genera, *in* Vassallo, A., and Antonucci, D., eds., Biology of Caviomorph Rodents: Diversity and Evolution (SAREM series A, Investigaciones Mastozoológicas): Buenos Aires, Sociedad Argentina para el Estudio de los Mamíferos (SAREM), p. 63–120.
Verzi, D.H., Álvarez, A., Olivares, A.I., Morgan, C.C., and Vassallo, A.I., 2010, Ontogenetic trajectories of key morphofunctional cranial traits in South American subterranean ctenomyid rodents: Journal of Mammalogy, v. 91, no. 6, p. 1508–1516, https://doi.org/10.1644/09-MAMM-A-411.1.
Verzi, D.H., Olivares, A.I., and Morgan, C.C., 2014, Phylogeny and evolutionary patterns of South American octodontoids rodents: Acta Paleontologica Polonica, v. 59, p. 757–769, https://doi.org/10.4202/app.2012.0135.
Vucetich, M.G., 1989, Rodents (Mammalia) of the Lacayani fauna revisited (Deseadan, Bolivia): Comparison with new Chinchillidae and Cephalomyidae from Argentina: Bulletin du Muséum National d'Histoire Naturelle, v. 11, no. 4, p. 233–247.
Vucetich, M.G., and Ribeiro, A.M., 2003, A new and primitive rodent from the Tremembé Formation (late Oligocene) of Brazil, with comments on the morphology of the lower premolars of caviomorph rodents: Revista Brasileira de Paleontología, v. 5, p. 73–82.
Vucetich, M.G, and Verzi, D.H., 1996, A peculiar octodontoid (Rodentia, Caviomorpha) with terraced molars from the lower Miocene of Patagonia (Argentina): Journal of Vertebrate Paleontology, v. 16, no. 2, p. 297–302.
Vucetich, M.G., and Vieytes, E.C., 2006, A middle Miocene primitive octodontoid rodent and its bearing on the early evolutionary history of the Octodontoidea: Palaeontolographica, Abteilung A, v. 27, no. 1, p. 79–89, https://doi.org/10.1127/pala/277/2006/81.

https://doi.org/10.1017/jpa.2022.98 Published online by Cambridge University Press

Vucetich, M.G., Mazzoni, M.M., and Pardiñas J.F., 1993, Los roedores de la Formación Collón Cura (Mioceno Medio), y la Ignimbrita Pilcaniyeu: Cañadón del Tordillo, Neuquén: Ameghiniana, v. 30, p. 361–381.

Vucetich, M.G., Kramarz, A.G., and Candela, A.M., 2010a, Colhuehuapian rodents from Gran Barranca and other Patagonian localities: The state of the art, *in* Madden, R.H., Carlini, A.A., Vucetich, M.G., and Kay, R.F., eds., The Paleontology of Gran Barranca: Evolution and Environmental Change Through the Middle Cenozoic of Patagonia: Cambridge, UK, University of Cambridge Press, p. 193–205.

Vucetich, M.G., Vieytes, E.C., Pérez, M.E., and Carlini, A.A., 2010b, The rodents from La Cantera and the early evolution of caviomorphs in South America, *in* Madden, R.H., Carlini, A.A., Vucetich, M.G., and Kay, R.F., eds., The Paleontology of Gran Barranca: Evolution and Environmental Change through the Middle Cenozoic of Patagonia: Cambridge, UK, University of Cambridge Press, p. 193–215.

Vucetich, M.G., Arnal, M., Deschamps, C.M., Pérez, M.E., and Vieytes, E.C., 2015a, A brief history of caviomorph rodents as told by the fossil record, *in* Vassallo, A., and Antonucci, D., eds., Biology of Caviomorph Rodents: Diversity and Evolution (SAREM series A, Investigaciones Mastozoológicas): Buenos Aires, Sociedad Argentina para el Estudio de los Mamíferos (SAREM), p. 11–62.

Vucetich, M.G., Dozo, M.T., Arnal, M., and Pérez, M.E., 2015b, New rodents (Mammalia) from the late Oligocene of Cabeza Blanca (Chubut) and the first rodent radiation in Patagonia: Historical Biology, v. 27, no. 2, p. 236–257, https://doi.org/10.1080/08912963.2014.883506.

Wagner, A., 1845, Diagnosen einiger neuen Arten von Nagern und Handflüglern: Archiv für Naturgeschichte, v. 11, no. 1, p. 145–149.

Wahlert, J.H., 1974, The cranial foramina of protrogomorphous rodents: An anatomical and phylogenetic study: Bulletin of the Museum of Comparative Zoology, v. 146, p. 363–410.

Wahlert, J.H., 1985, Cranial foramina of rodents, *in* Luckett, W.P., and Hartenberger, J.-L., eds., Evolutionary Relationships Among Rodents: A multidisciplinary analysis: New York, Plenum Press, p. 311–332.

Wahlert, J.H., Korth, W.W., and McKenna, M.C., 2006, The skull of *Rapamys* (Ischyromyidae, Rodentia) and description of a new species from the Duchesnean (late middle Eocene) of Montana: Palaeontographica, Abteilung A, v. 26, p. 39–51, https://doi.org/10.1127/pala/277/2006/39.

Waterhouse, G.R., 1848, A Natural History of the Mammalia: Rodentia, or Gnawing Mammalia, Volume 2: London, Hippolyte Baillière, 500 p., 22 pls.

Wible, J.R., 1987, The eutherian stapedial artery: Character analysis and implications for superordinal relationships: Zoologica Journal of the Linnean Society, v. 91, p. 107–135.

Wible, J.R., and Shelley, S.L., 2020, Anatomy of the petrosal and middle ear of the brown rat, *Rattus norvegicus* (Berkenhout, 1769) (Rodentia, Muridae): Annals of the Carnegie Museum, v. 86, no. 1, p. 1–35, https://doi.org/10.2992/007.086.0101.

Wied-Neuwied, M.P. zu, 1820, Ueber ein noch unbeschriebenes Säugethier aus der Familie der Nager: Isis von Oken, v. 6, p. 43.

Wilson, R.W., 1940, Californian paramyid rodents: Carnegie Institution of Washington Contributions to Paleontology, v. 514, p. 59–83.

Wilson, R.W., 1949, On some White River fossil rodents, *in* Some Tertiary Mammals and Birds from North America: Washington, D.C., Carnegie Institution of Washington (Publication no. 584), p. 27–50.

Wood, A.E., 1955, A revised classification of the rodents: Journal of Mammalogy, v. 36, no. 2, p. 165–187.

Wood, A.E., 1962, The early Tertiary rodents of the family Paramyidae: Transactions of the American Philosophical Society, v. 52, p. 1–261.

Wood, A.E., 1968, Early Cenozoic mammalian faunas, Fayum Province, Egypt, Part 2, The African Oligocene Rodentia: Bulletin of Peabody Museum of Natural History, v. 28, p. 23–105.

Wood, A.E., and Patterson, B., 1959, The rodents of the Deseadan Oligocene of Patagonia and the beginnings of South American rodent evolution: Bulletin of the Museum of Comparative Zoology, v. 120, p. 281–428.

Yao, L., Brown, J.P., Stampanoni, M., Marone, F., Isler, K., and Martin, R.D., 2012, Evolutionary change in the brain size of bats: Brain, Behavior and Evolution, v. 80, p. 15–25, https://doi.org/10.1159/000338324.

Zimmermann, E.A.W., 1780, Geographische Geschichte der Menschen, und der algemein verbreiteten vierfüssigen Thiere, Volume 2: Leipzig: Wenganschen Buchhandlung, 432 p.

Accepted: 18 October 2022